Electronic Supplementary Material (ESI) for Journal of Materials Chemistry A.
This journal is © The Royal Society of Chemistry 2016

Mechanochemically Synthesized Covalent Organic Framework as Proton-conducting Solid Electrolyte

Digambar Balaji Shinde,[a,‡] Harshitha Barike Aiyappa,[a,b,‡] Mohitosh Bhadra,[a,b, ‡] Bishnu P. Biswal,[a,b] Pritish Wadge,[a] Sharath Kandambeth,[a,b] Bikash Garai,[a,b] Tanay Kundu,[a,b]* Sreekumar Kurungot[a,b]* and Rahul Banerjee[a,b]*

[a]Physical/Materials Chemistry Division, CSIR- National Chemical Laboratory, Dr. Homi Bhabha Road, Pune 411008, India.
[b]Academy of Scientific and Innovative Research (AcSIR), New Delhi, India

Supporting Information

Section S-1: General Information

General Remarks: All other reagents and solvents were commercially available and used as received. Powder X-ray diffraction (PXRD) patterns were recorded on a Rigaku, MicroMax-007HF with high intensity Micro focus rotating anode X-ray generator. All the samples were recorded in the 2θ range of 2–40 degrees and data was collected with the help of Control Win software. A Rigaku, R-axis IV++ detector was employed in wide-angle experiments. The radiation used was CuK (1.54 Å) with a Ni filter, and the data collection was carried out using an Aluminium holder. Fourier transform infrared (FT-IR) spectra were taken on a Bruker Optics ALPHA-E spectrometer with a universal Zn-Se ATR (Attenuated Total Reflection) accessory in the 600-4000 cm^{-1} region or using a Diamond ATR (Golden Gate). Thermogravimetric analyses (TGA) were carried out on a TG50 analyzer (Mettler-Toledo) or a SDT Q600 TG-DTA analyzer under N_2 atmosphere at a heating rate of 10 ºC min^{-1} within a temperature range of 30-900 °C. SEM images were obtained with a Zeiss DSM 950 Scanning Electron Microscope and FEI, QUANTA 200 3D Scanning Electron Microscope with tungsten filament as electron source operated at 10 kV. The samples were sputtered with Au (nano-sized film) prior to imaging by a SCD 040 Balzers Union. TEM images were recorded using FEI Tecnai G2 F20 X-TWIN TEM at an accelerating voltage of 200 kV. The TEM Samples were prepared by drop casting the sample from 2-propanol on copper grids TEM Window (TED PELLA, INC. 200 mesh). All gas adsorption experiments (0 to 1 bar) were performed on a Quantachrome *Quadrasorb* automatic volumetric instrument. Solid state NMR (SSNMR) was taken in a Bruker 300 MHz NMR spectrometer and ligand NMR data were taken in Bruker 300 MHz NMR spectrometer. ^{31}P CPMAS NMR spectra were recorded with Bruker AVENCE 300 MHz Spectrometer equipped with 4-mm double-resonance probe, operating at 300.00 MHz for ^1H and 121.442 MHz for ^{31}P. Typical NMR experimental conditions were as follows $\pi/2$ duration, 2μs; recycle delay, 5s; spinning speed, 10 KHz. Chemical shift externally referenced to ortho-phosphoric acid at 0.0 ppm. The UV-VIS spectra were recorded using Carry Win 50 (Agilent Tech.) after dissolving the materials in chloroform or acetonitrile-water medium.

Section S-2: Synthetic procedures

Synthesis of 1,3,5-triformylphloroglucinol (Tp):

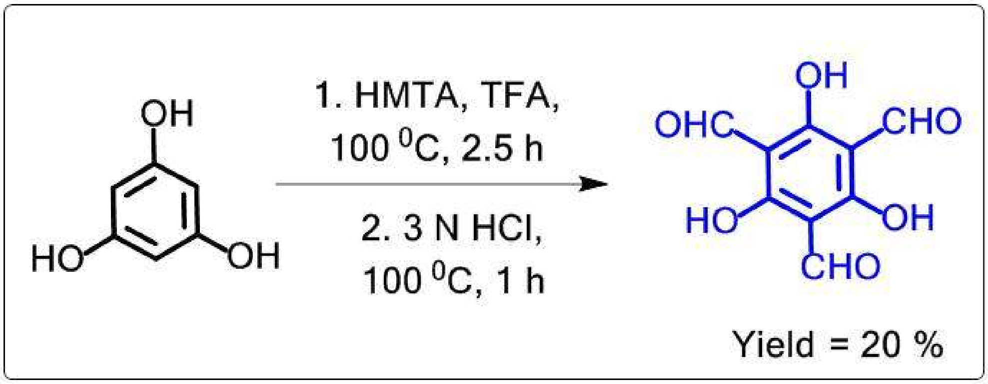

The 1,3,5-triformylphloroglucinol was prepared using reported literature procedure and their characterizations matched well with that of literature data reported earlier.[1]

Synthesis of 5-Amino-2,2'-bipyridine (4):

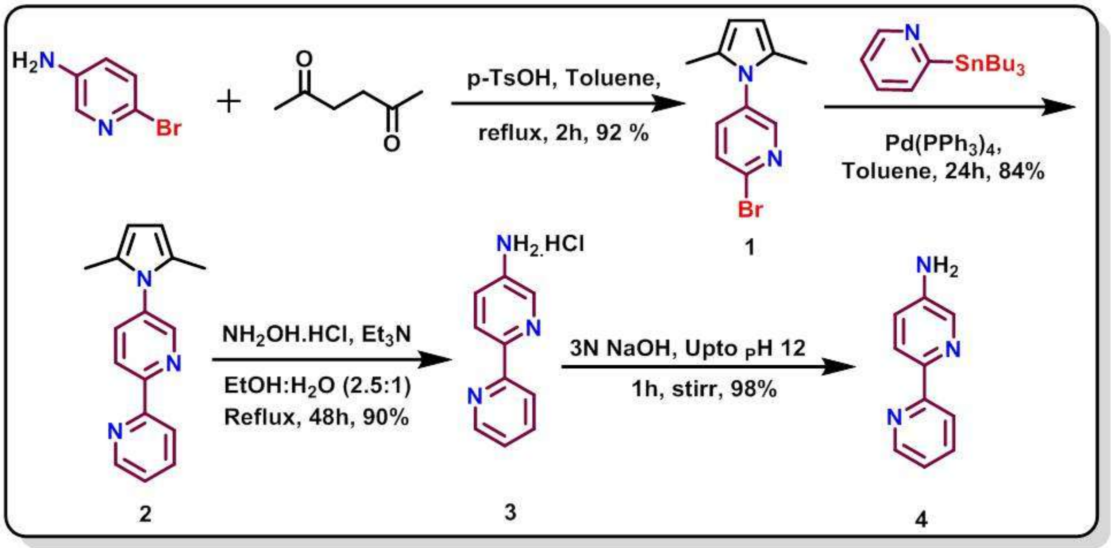

These compounds 1-(2-Bromopyridine-5-yl)-2,5-dimethyl-1H-pyrrole (**1**), 1-(2,2'-Bipyridine-5-yl)-2,5-dimethyl-1H-pyrrole (**2**) and 5-Amino-2,2'-bipyridine (**4**) were synthesized using reported methods and confirmed by IR, ^{1}HNMR, and ^{13}C NMR.[2]

Synthesis of 2,2'-bipyridine-5,5'-diamine (Bpy):

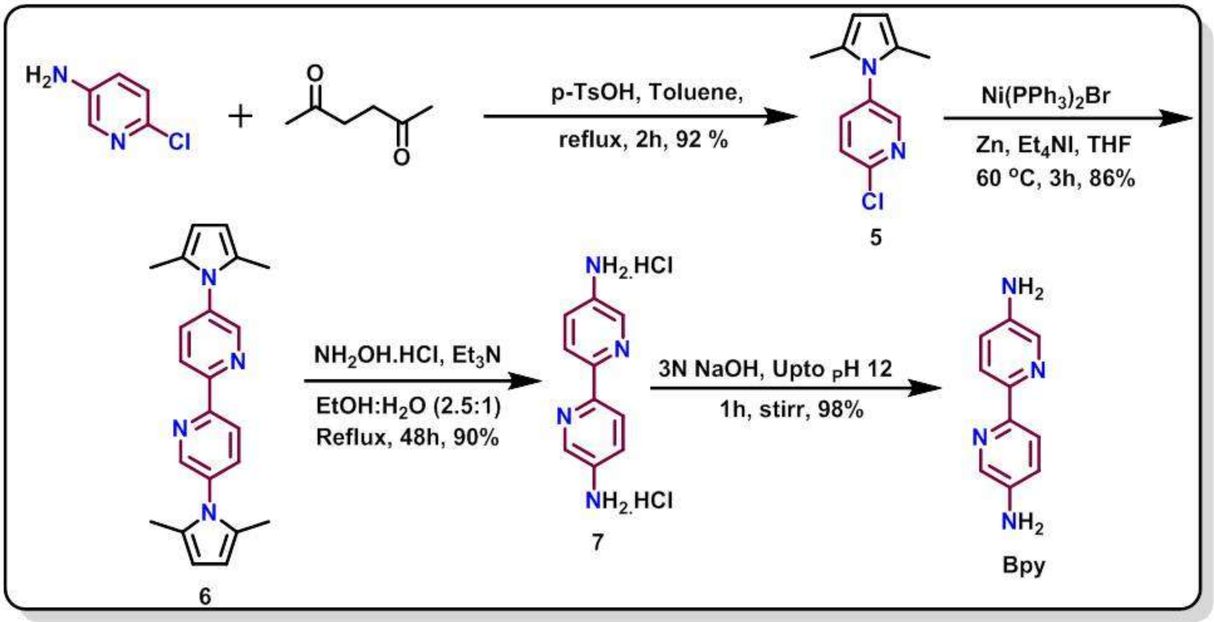

These compounds, 1-(2-Chloropyridine)-5-yl-2,5-dimethyl-1H-pyrrole (**5**), 5,5’-Bis(2,5-dimethyl-1H-pyrrole)-2,2’-bipyridine (**6**), and 2,2'-bipyridine-5,5'-diamine (**Bpy**) were synthesized using reported methods and confirmed by IR, ^{1}HNMR, and ^{13}CNMR.

Monomer Synthesis : *(2E,4E,6E)-2,4,6-tris(([2,2'-bipyridin]-5-yl-amino)methylene)cyclohexane-1,3,5-trione*.

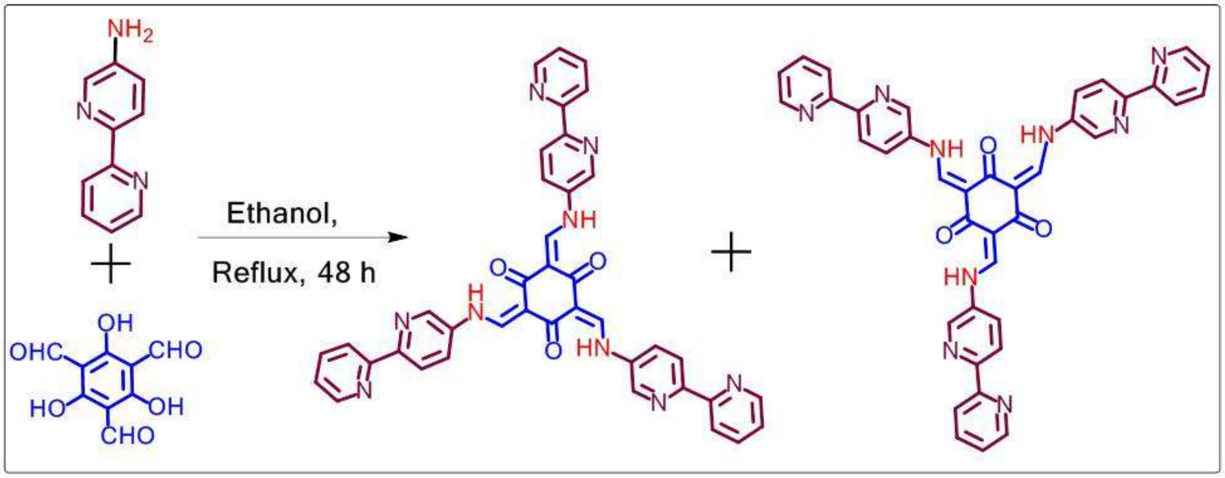

The monomer was synthesized by the reaction between 1,3,5-triformylphloroglucinol (**Tp**) (0.105 g, 0.5 mmol) and 5-Amino-2,2’-bipyridine (0.370 g, 2.0 mmol) in 25 mL of ethanol under refluxing condition for 48 h. After that, the solution was cooled to room temperature and then precipitate was collected by filtration, washed with copious amount of ethanol, and finally dried under vacuum to give 0.274 g (82%) of a yellow solid.[3]

FT-IR (powder):υ_{max} 1610,1565,1447,1396,1207,1095,991,826,731,640; **^{1}H NMR (300 MHz, $CDCl_3$)**: δ 7.27-7.42 (m, 6H), 7.90-7.73 (m, 24H), 8.42-8.40 (m, 6H), 8.62-8.60 (m, 6H), 8.78 (d, J = 12.3 Hz, 2H), 8.92 (d, *J* = 12.3 Hz, 1H) 9.95 (d, J = 12.3 Hz, 3H), 13.19 (d, *J* = 12.3 Hz, 3H), 13.60 (d, *J* = 12.3 Hz, 2H), 13.80 (d, *J* = 12.3 Hz, 1H).

TpBpy-ST (Solvothermal Route): A pyrex tube (o.d. × i.d. = 18 × 10 mm^2 and length 16 cm) is charged with 1,3,5-triformylphloroglucinol (**Tp**) (63.0 mg, 0.3) and 2,2'-bipyridine-5,5'-diamine (**Bpy**) (83.7 mg, 0.45 mmol) and 4.5 mL of dimethylacetamide (DMAc) and 1.5 mL of o-dichlorobenzene (o-DCB), 0.6 mL of 6.0 M aqueous acetic acid (AcOH). This mixture was sonicated for 10-15 minutes in order to get a homogenous dispersion. The tube was then flash frozen at 77 K (liquid N_2 bath) and degassed by three freeze-pump-thaw cycles. The tube was sealed off and then heated at 120 °C for 3 days. A dark red colored precipitate formed was collected by centrifugation or filtration and washed with 5-6 times with dimethylacetamide (DMAc), water and then acetone. The powder collected was then solvent exchanged with acetone three times and then dried at 150 °C under vacuum for 24 h to give a dark red colored powder in □ 79 % isolated yield. The elemental micro analysis (C, N, H) of the **TpBpy-ST**, the experimental data are very well matched with the theoretical one, indicating the purity of the material.

FT-IR (powder): υ_{max} 1607,1579,1458,1397,1270,1095,992,826,732,640. Elemental analysis (%) calcd. for $(C_8H_6N_2O)_n$ C (65.75), H (4.14), N (19.17), found C (66.84), H (4.21), N (18.69).

TpBpy-MC (Mechanochemical Route): 1,3,5-triformylphloroglucinol (**Tp**) (63.0 mg, 0.3) and 2,2'-bipyridine-5,5'-diamine (**Bpy**) (83.7 mg, 0.45 mmol) was placed in a 5 mL stainless steel jar, with one 7 mm diameter stainless steel ball, ~60 µL of DMAc, ~30 µL of o-DCB and ~15 µL of 6 M acetic acid. The synthesis was tried at different ball milling time and frequency (**Table S1**). In an optimized procedure, the reaction mixture was ground for 90 min at 30 Hz, followed by its washing with minimal amount of DMAc followed by copious amount of water and acetone. The powder then collected and solvent exchanged with acetone about three times and then dried at 150 °C under vacuum for 24 h to give a red colored powder in 84 % isolated yield. The elemental analysis and FT-IR peaks of COFs **TpBpy-MC** were matched well with **TpBpy-ST,** synthesized using the solvothermal route.

Table S1. Different milling frequency, time for the synthesis of TpBpy-MC.

Condition	Time (min)	Frequency (Hz)	Yield (%)	BET Surface Area ($m^2 g^{-1}$)	Proton conductivity ($S\ cm^{-1}$)
LAG	**30**	**30**	**52**	**~ 59**	**0.82×10^{-4}**
LAG	**60**	**30**	**76**	**~ 219**	**1.83×10^{-3}**
LAG	**90**	**30**	**84**	**~ 293**	**2.5×10^{-3}**
LAG	**120**	**30**	**84**	**~ 293**	**2.63×10^{-3}**
LAG	**120**	**20**	**68**	**~156**	**2.14×10^{-3}**
Neat	**120**	**30**	**72**	**~ 72**	**0.42×10^{-4}**

The optimization of COF mechanosynthetic conditions was performed by varying the milling frequency and milling time. The PXRD spectral comparison revealed that resulting samples needed a minimal of 60 min milling (30 Hz) for the formation of COFs. Of all, by the virtue of their high surface area and minimal ball milling time, the samples milled for 90 min was chosen for phosphoric acid loading and was thereafter tested for their proton conducting ability.

Section S-3: Structural modeling and powder X-ray diffraction analysis

Atomic positions and cell sizes of modeled COF layers were optimized using Self-Consistent Charge Density Functional Tight-Binding (SCC-DFTB) Method. Stacking of layers are affected by the Coulomb repulsion between the partial atomic charges in adjacent layers.[4] Hence, we performed Mulliken population analysis for the charges. The adjacent layers were shifted with respect to each other in different directions in order to avoid Coulomb repulsion from charges alike. Several possibilities were considered, however, the best was taken from comparison of simulated PXRD pattern with the experimental. Inter layer separation was also determined from the comparison of PXRD patterns. The fractional coordinates of **TpBpy** are given in **Table S2**.

In order to elucidate the structure of these COFs and to calculate the unit cell parameters, possible 2-D models were optimized using Density Functional Tight-Binding method. Several stacking possibilities were considered for reasons reported in the literature. The experimental PXRD patterns are agreeable with the simulated patterns of some near-eclipsed stacking models (Figure S1, S2 and S3). Hence we propose structures close to hexagonal space group (*P*6) for **TpBpy** by comparing the experimental and simulated PXRD patterns. Refinements of PXRD pattern were done using Reflex module of Material Studio.[5]

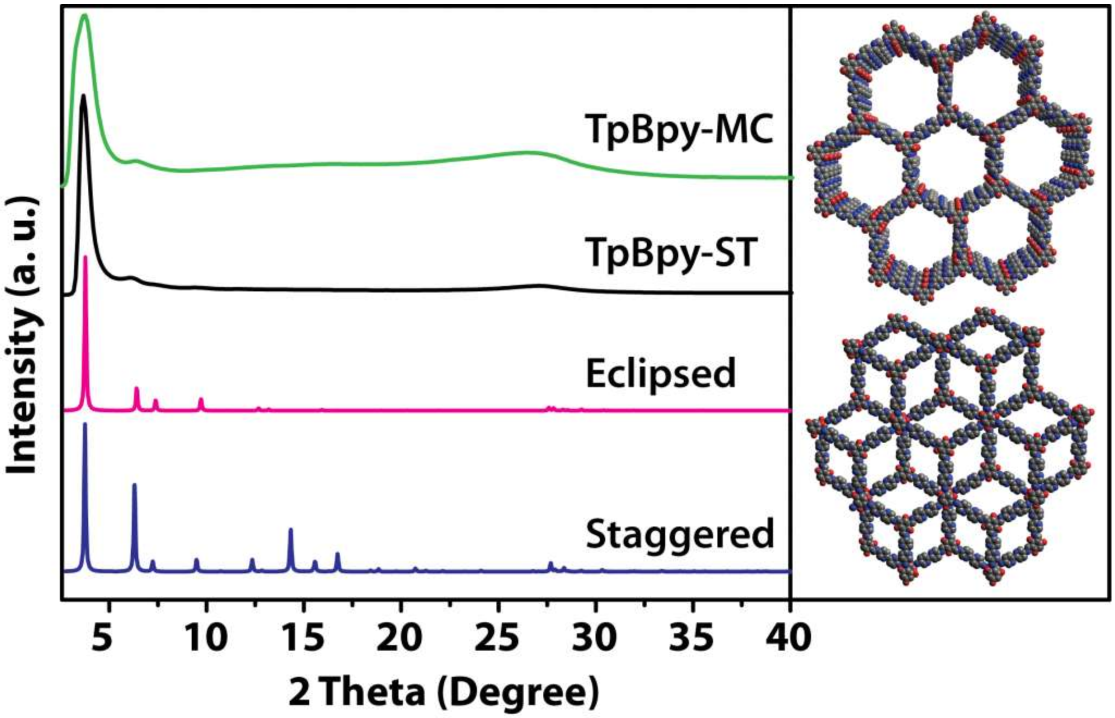

Figure S1: PXRD patterns of as-synthesized **TpBpy-ST** (Black) and **TpBpy-MC** (Green) compared with the eclipsed (Pink) and staggered (Blue) stacking models.

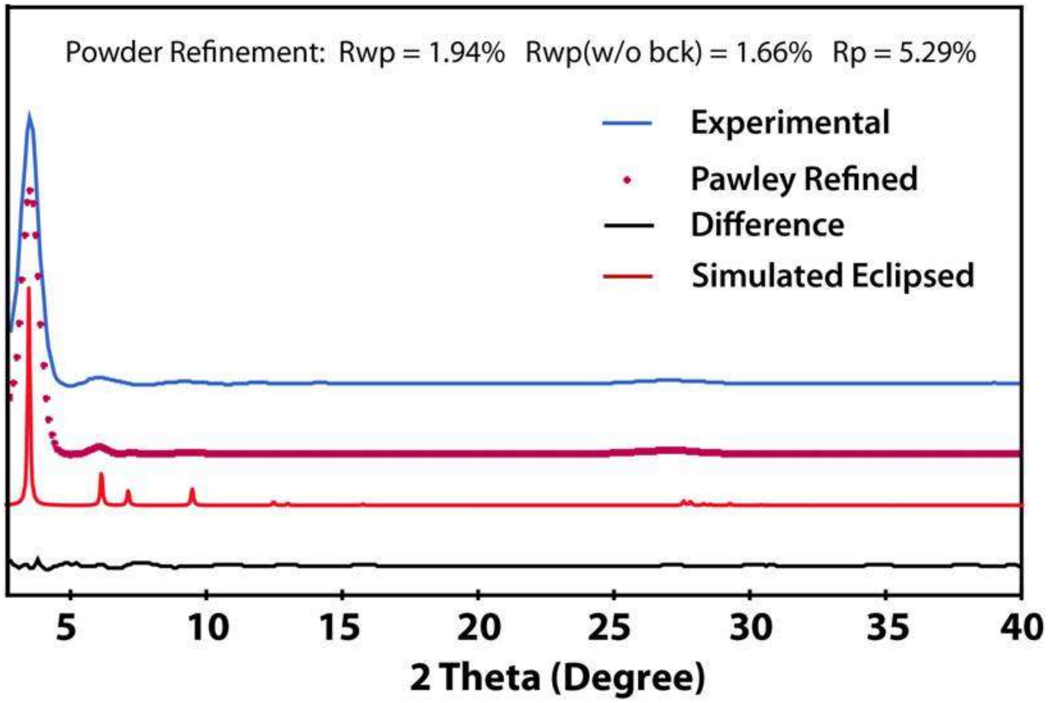

Figure S2: Experimental (Blue) compared with Pawley refined (Wine) PXRD profiles of **TpBpy-ST** with a simulated eclipsed (Red) and difference plot is given in (Black).

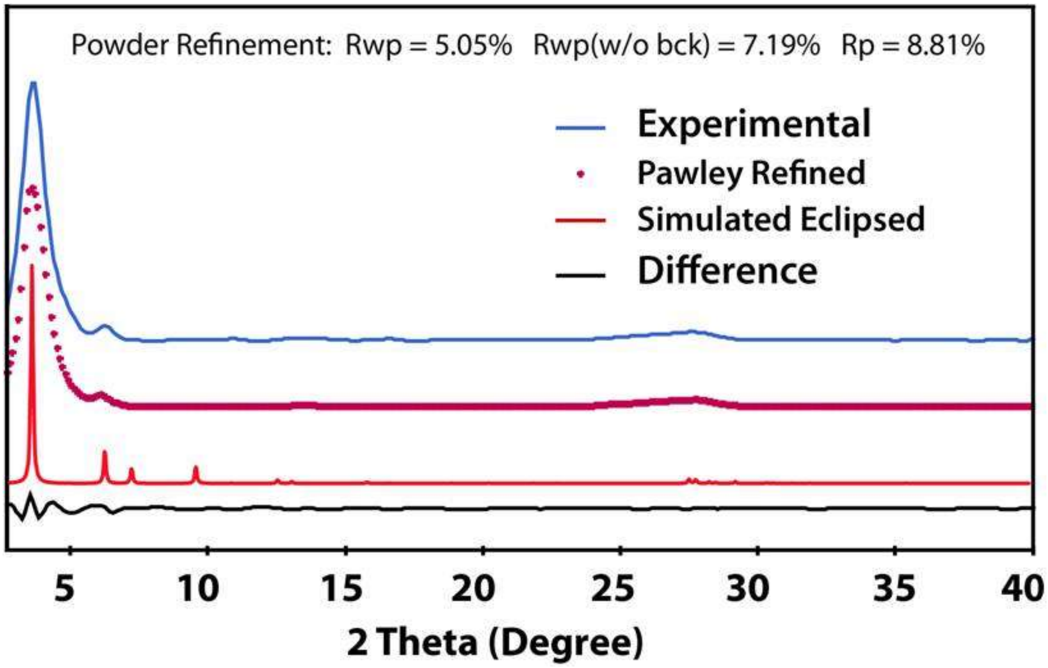

Figure S3: Experimental (Blue) compared with Pawley refined (Wine) PXRD profiles of **TpBpy-MC** with a simulated eclipsed (Red) and difference plot is given in (Black).

Table S2. Fractional atomic coordinates for the unit cell of TpBpy

TpBpy			
Hexagonal, *P6/m* a= b= 29.3 Å, , c= 3.5 Å *α* = 90.0°, *β* = 90.0°, *γ* = 120°			
C1	0.51519	0.49086	0.47194
C2	0.56958	0.52323	0.46886
C3	0.60194	0.50122	0.46782
C4	0.57993	0.44683	0.46986
C5	0.52555	0.41446	0.47293
N1	0.49318	0.43648	0.47397
N2	0.61501	0.42795	0.46881
C6	0.63085	0.35423	0.46981
C7	0.59597	0.37453	0.47085
C8	0.61035	0.29759	0.47184
O1	0.55671	0.26495	0.47492

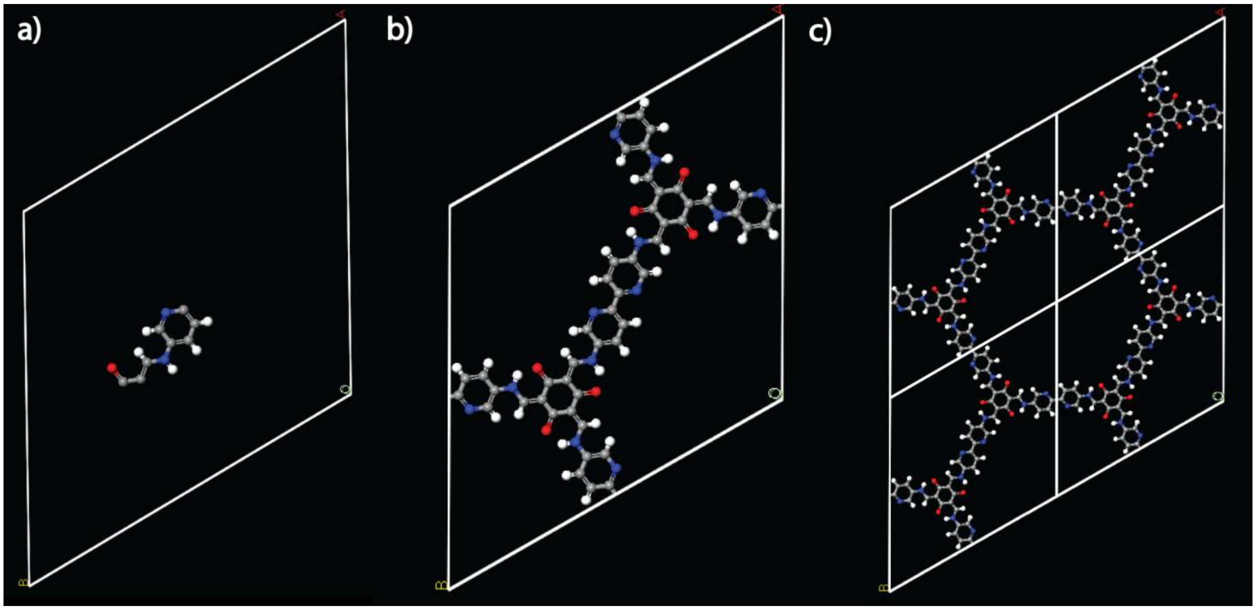

Figure S4: (a) Asymmetric unit, (b) Unit cell and (c) Eclipsed crystal lattice packing of COF **TpBpy**.

Section S-4: FT-IR Spectra

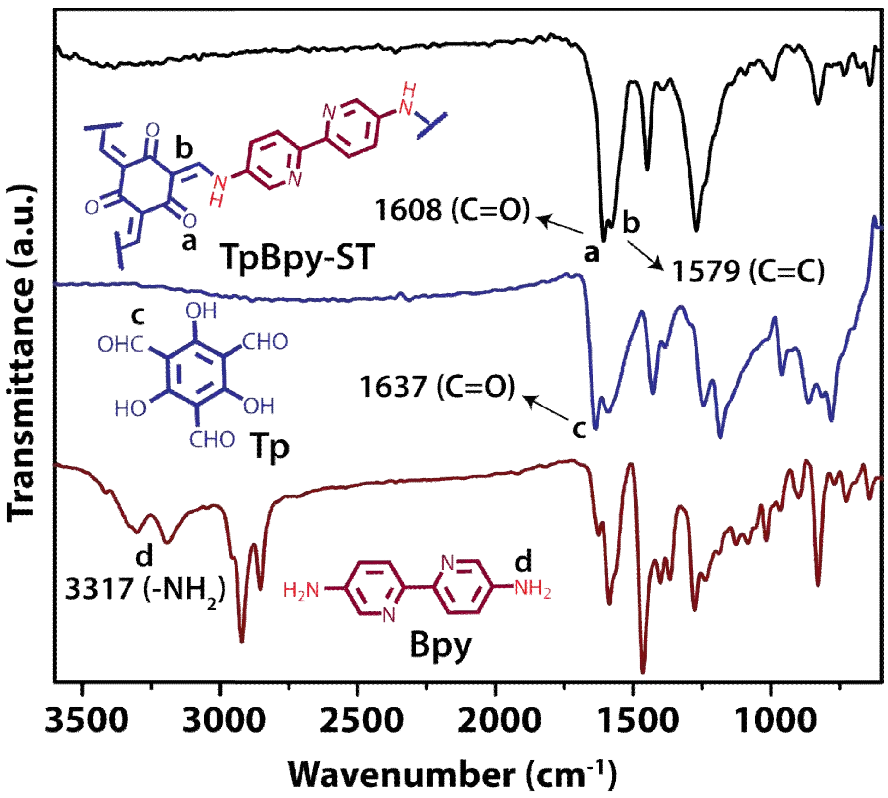

Figure S5: FT-IR spectra of **TpBpy-ST** (Black), 1,3,5-triformylphloroglucinol (**TP**, Blue) and 2,2’-bipyridine-5,5'-diamine (**BPy**, Brown).

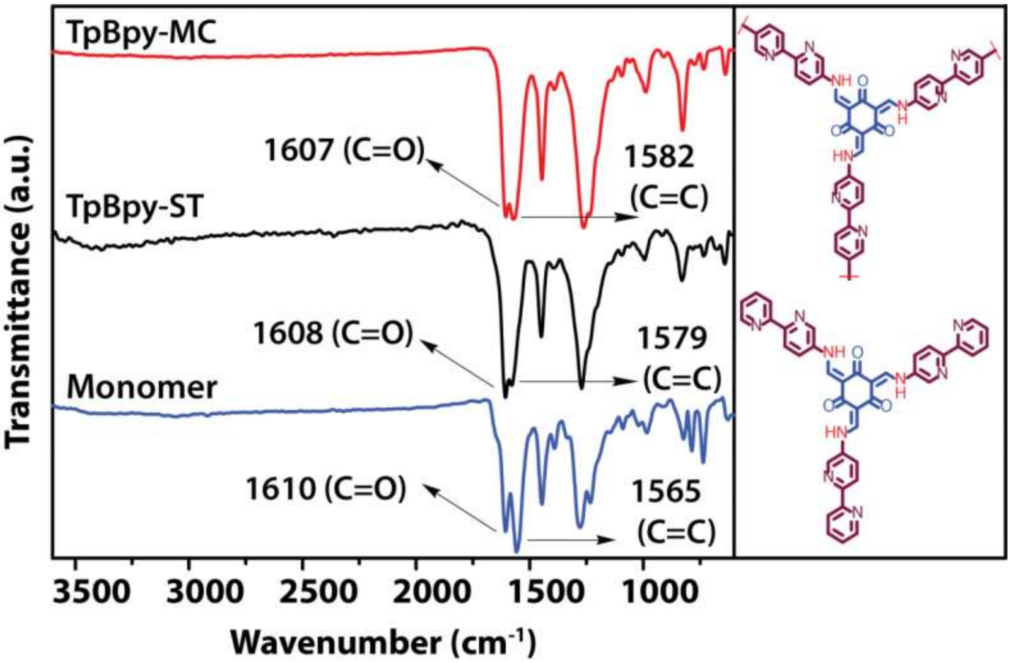

Figure S6: FT-IR spectra of **TpBpy-MC** (Red), **TpBpy-ST** (Black) and monomer (Blue).

Section S-5: ^{13}C CP/MAS NMR Spectra

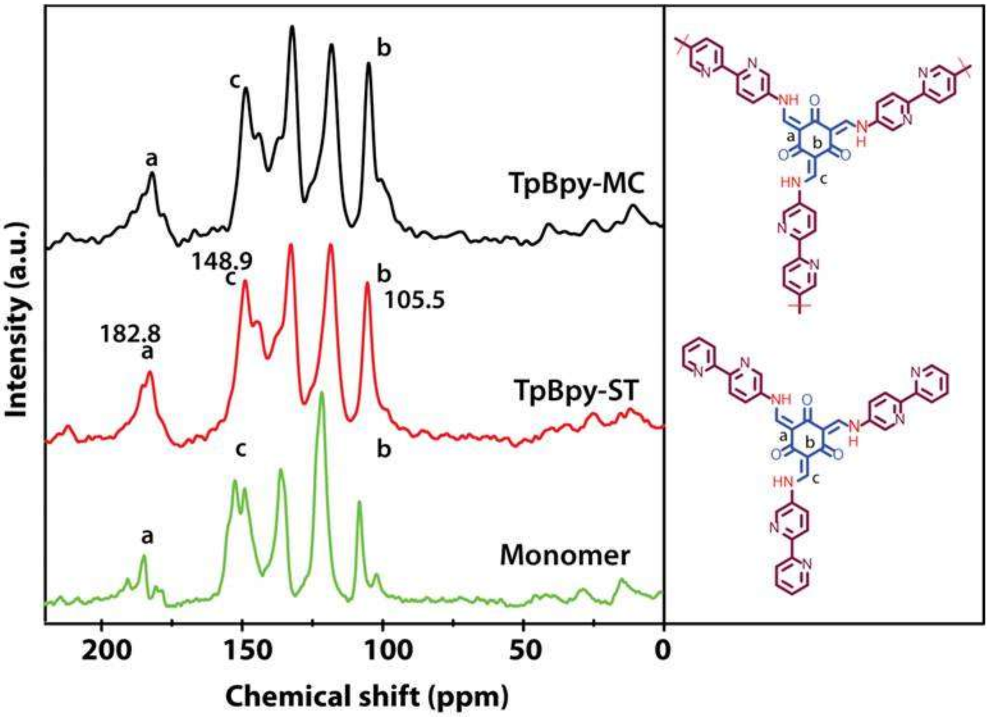

Figure S7: ^{13}C CP-MAS spectrum of **TpBpy-MC** (Black), **TpBpy-ST** (Red) and monomer (Green).

Section S-6: Scanning Electron Microscopy (SEM)

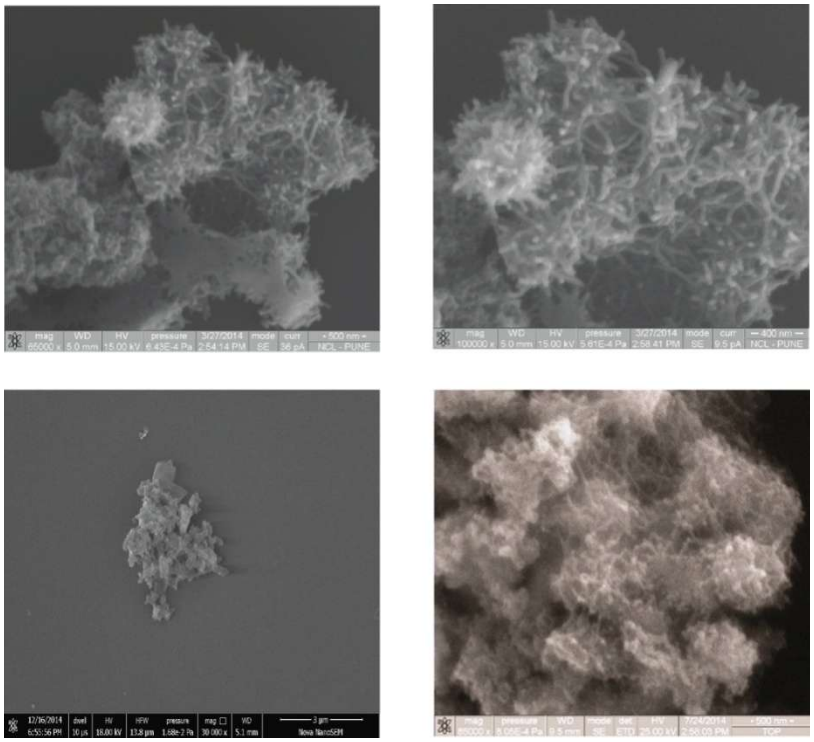

Figure S8: SEM images of **TpBpy-ST**

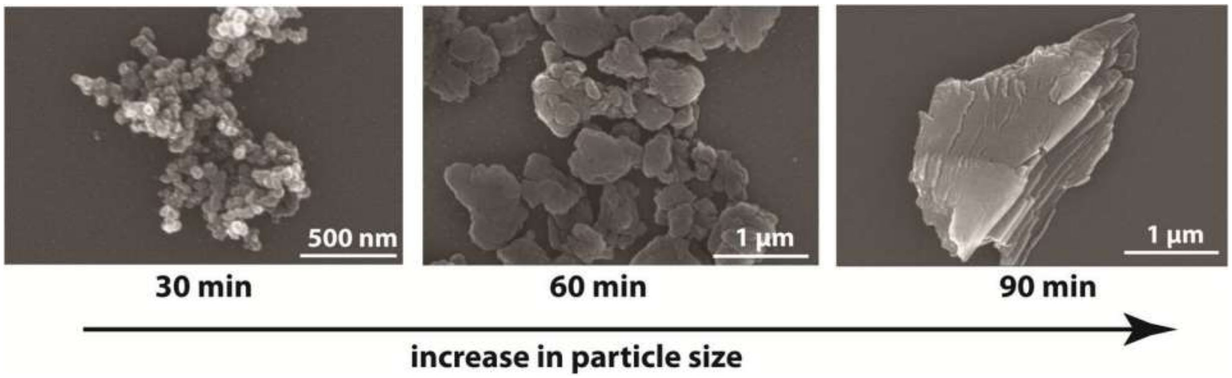

Figure S9: SEM images of mechanochemically synthesised **TpBpy-MC** at regular milling time interval at 30 Hz milling frequency.

Section S-7: Transmission Electron Microscopy (TEM)

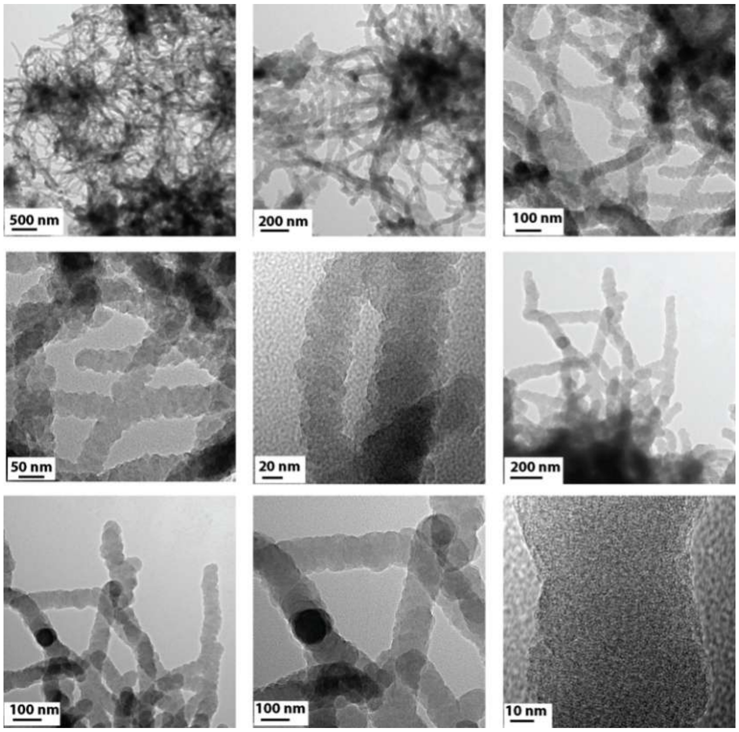

Figure S10: TEM images of **TpBpy-ST**.

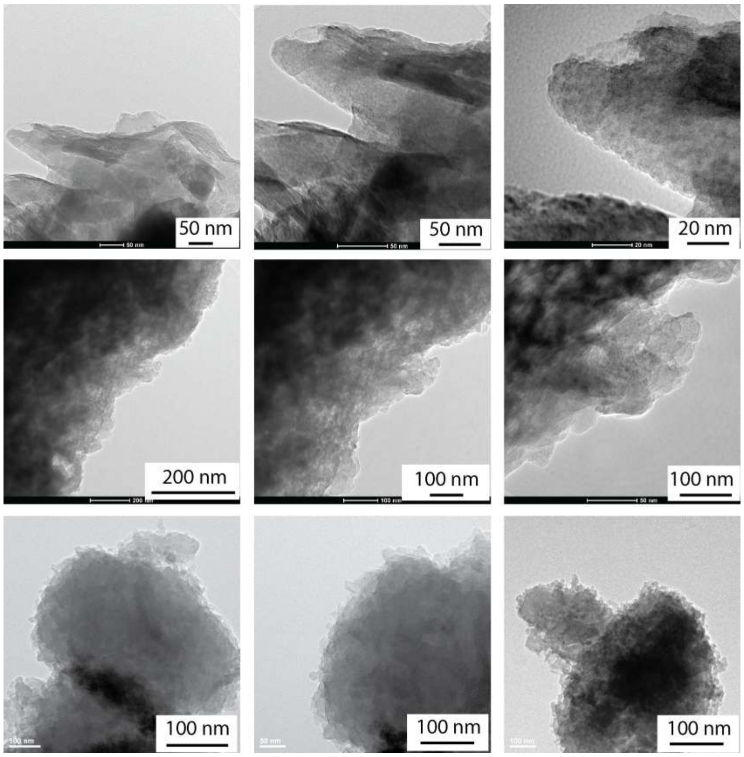

Figure S11: **TEM** images of **TpBpy–MC**.

Section S-8: Thermo Gravimetric Analysis (TGA)

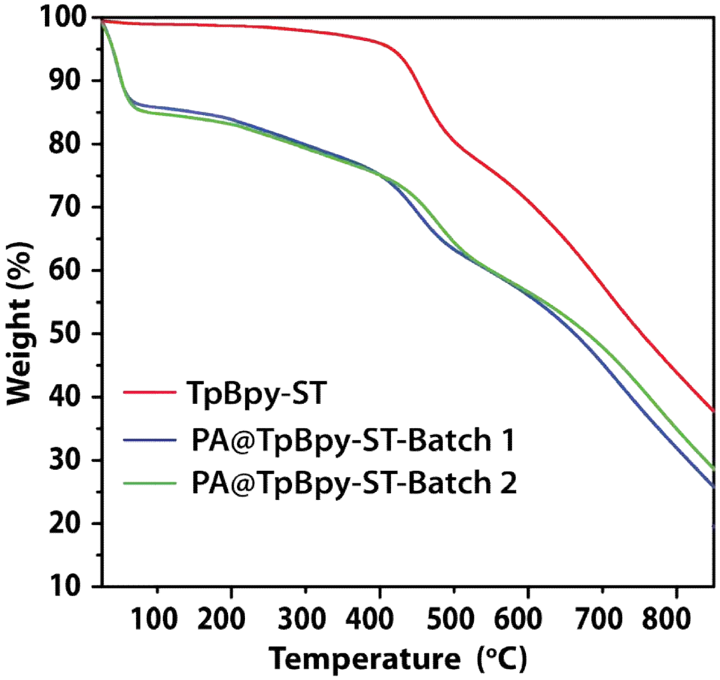

Figure S12: TGA data of COF **TpBpy-ST** (Red) and **PA@TpBpy-ST-Batch-1, 2** (Blue, Green) under N_2 atmosphere.

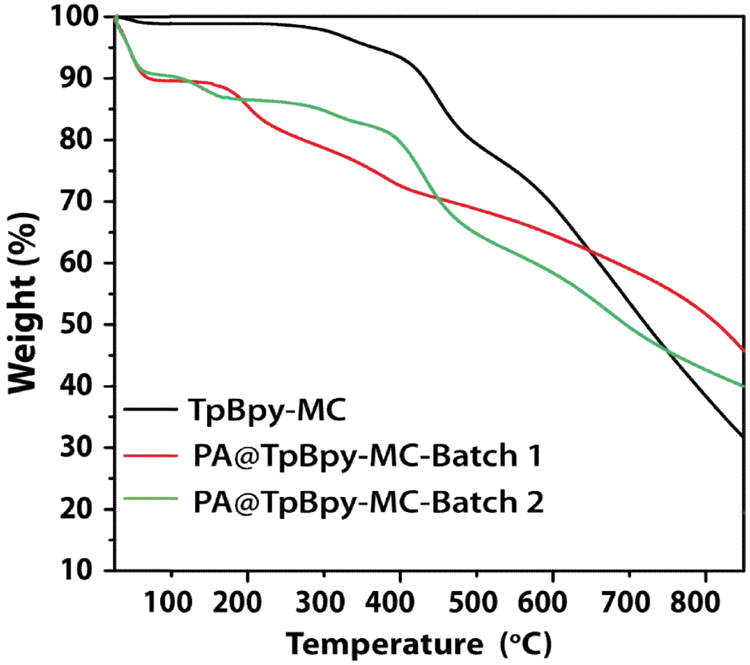

Figure S13: TGA data of COF **TpBpy-MC** (Black) and **PA@TpBpy-MC-Batch-1, 2** (Red, Green) under N_2 atmosphere.

Section S-9: Gas adsorption studies of TpBpy

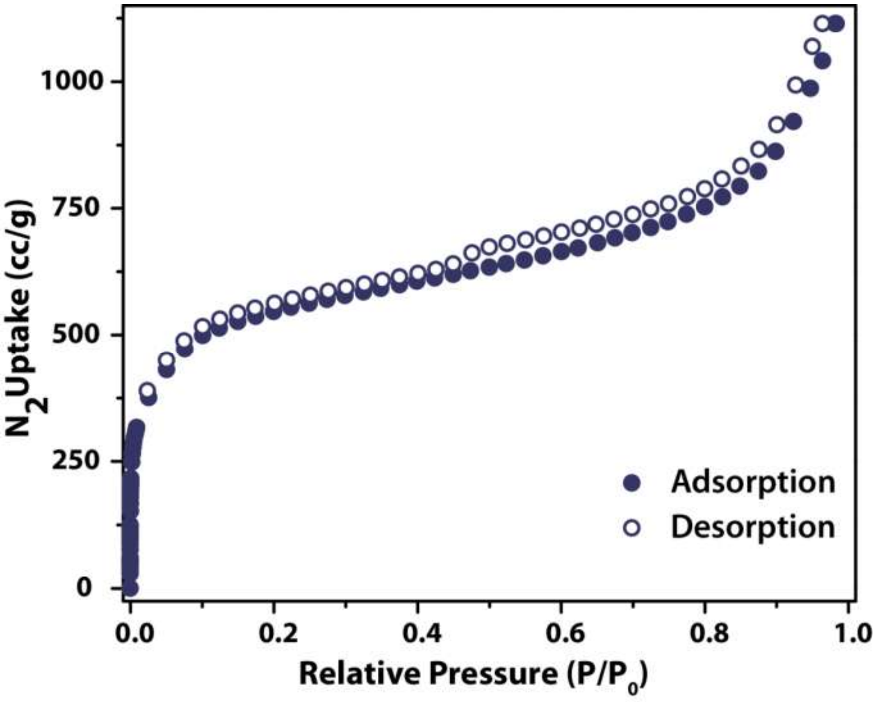

Figure S14: N_2 adsorption isotherms of **TpBpy-ST**.

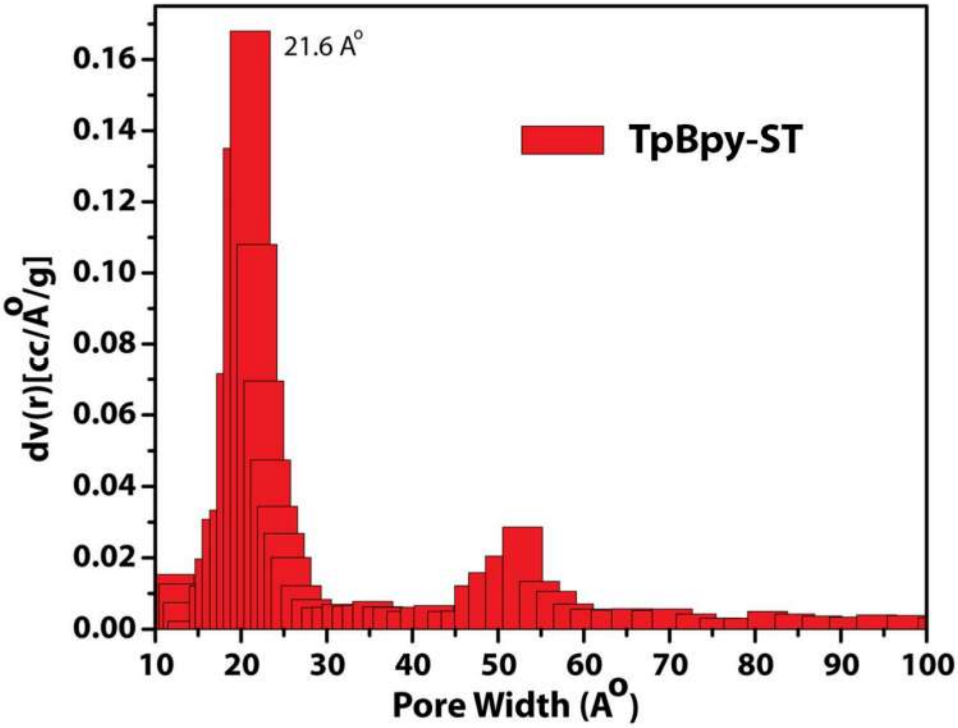

Figure S15: Pore size distribution of **TpBpy-ST** (measured by using NLDFT method).

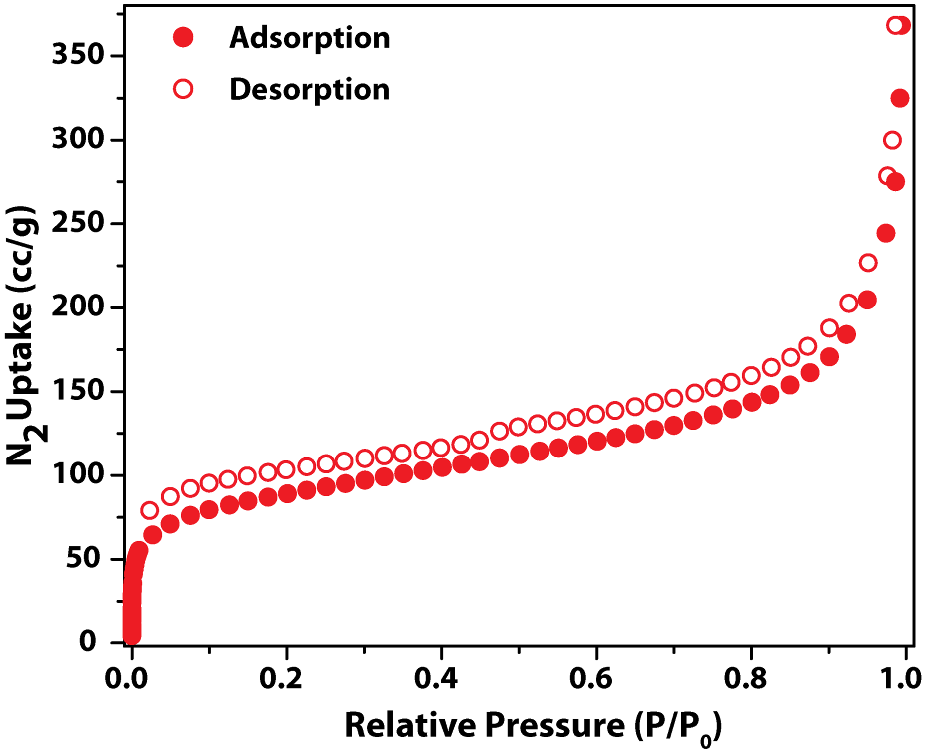

Figure S16: N_2 adsorption isotherms of **TpBpy-MC** at milling frequency 30 Hz and milling time 90 min.

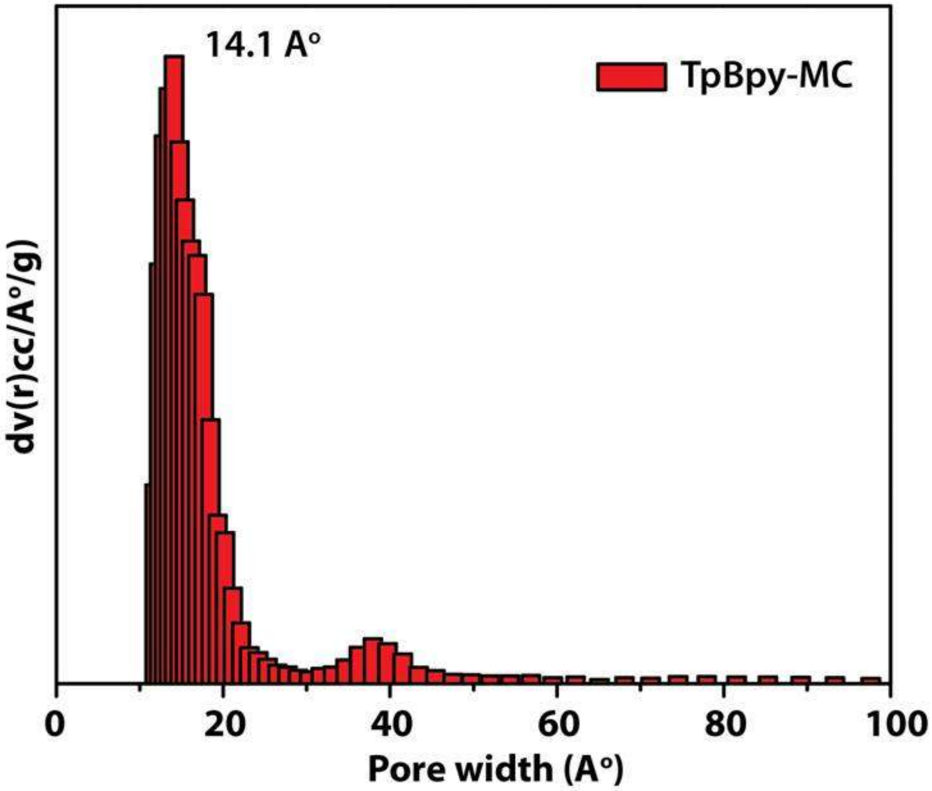

Figure S17: Pore size distribution of **TpBpy-MC** (Measured by using NLDFT method).

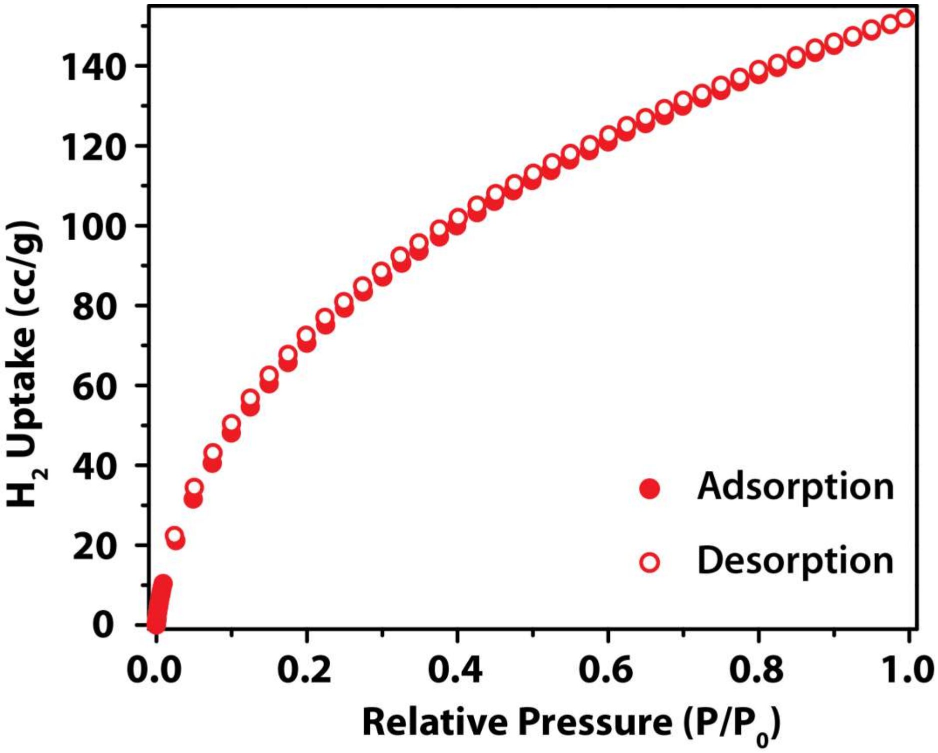

Figure S18: Hydrogen adsorption isotherms of **TpBpy-ST** at 77 K.

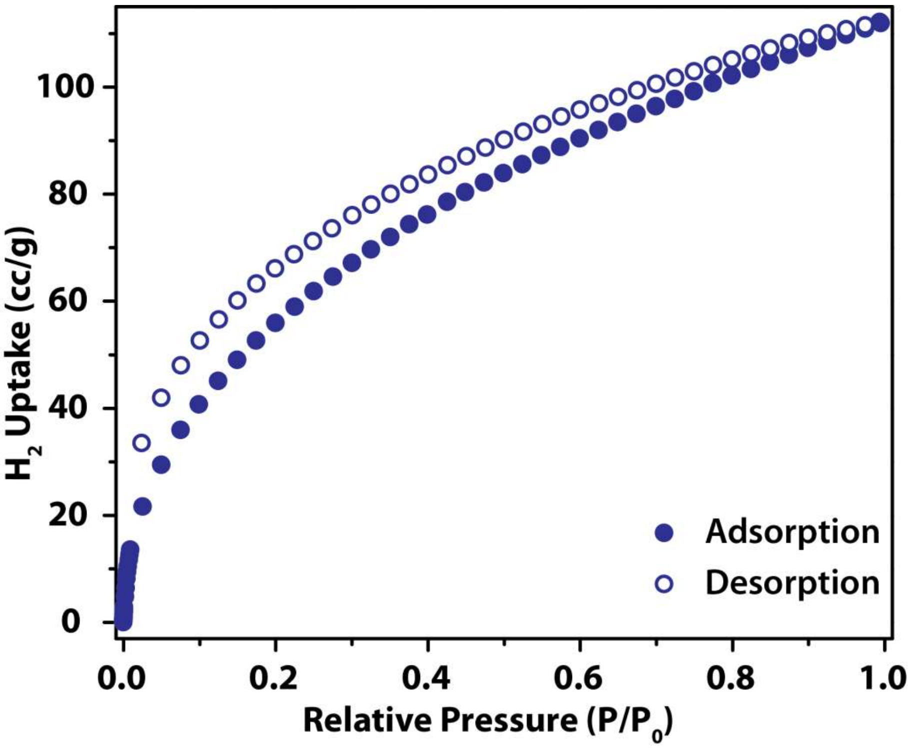

Figure S19: Hydrogen adsorption isotherms of **TpBpy-MC** at 77 K.

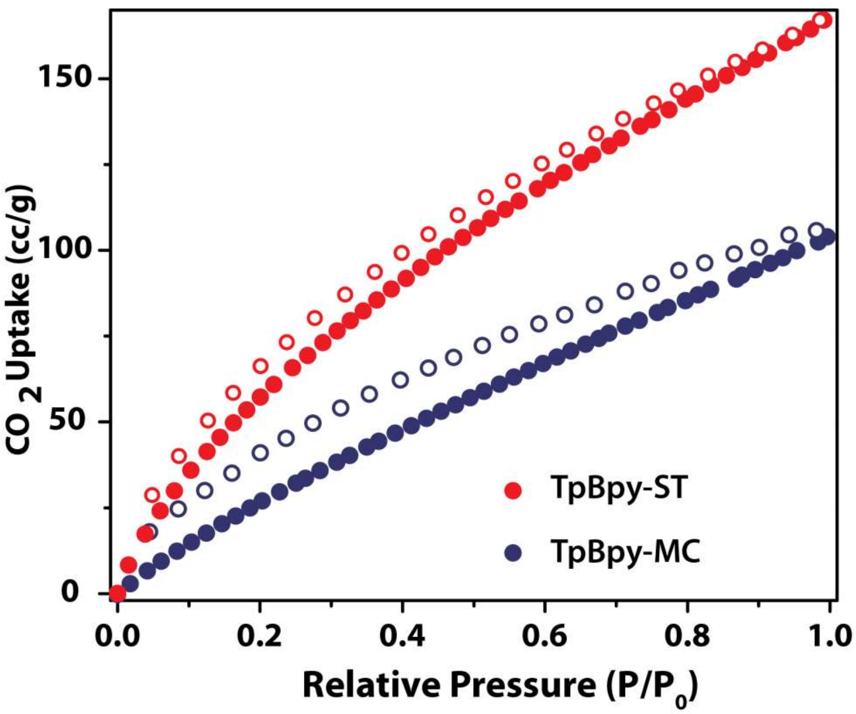

Figure S20: Carbon dioxide adsorption isotherms of **TpBpy-ST** (Red) and **TpBpy-MC** (Blue) at 0 ºC.

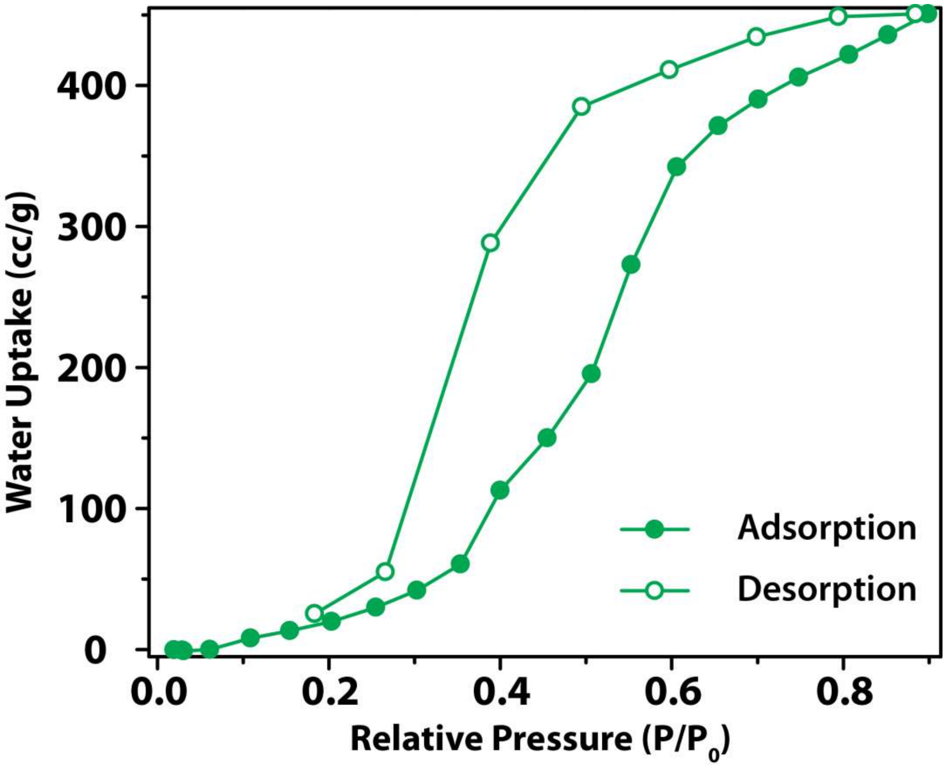

Figure S21: Water adsorption isotherms of **TpBpy-ST**.

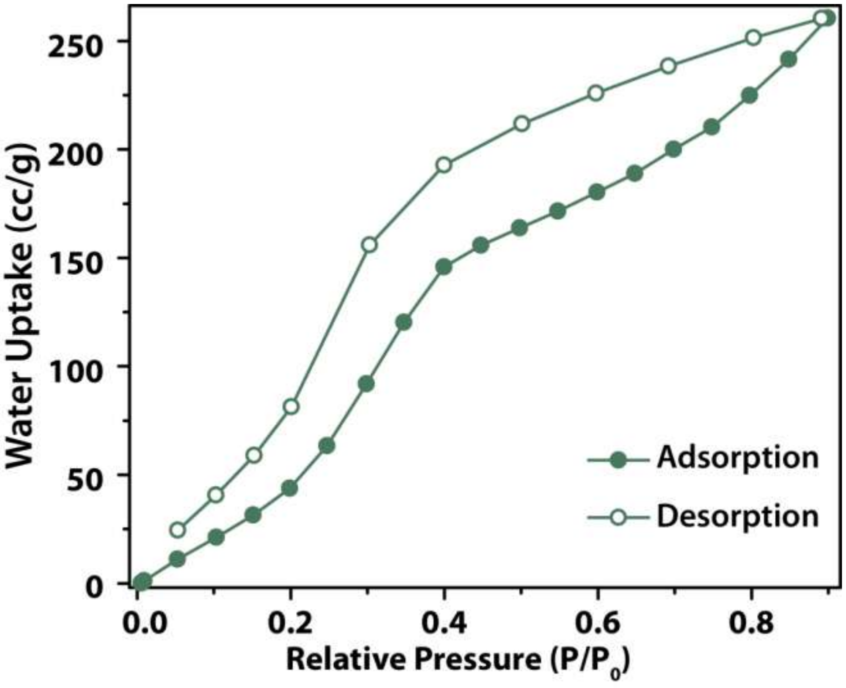

Figure S22: Water adsorption isotherms of **TpBpy-MC**.

Section S-10: Stability studies of TpBpy

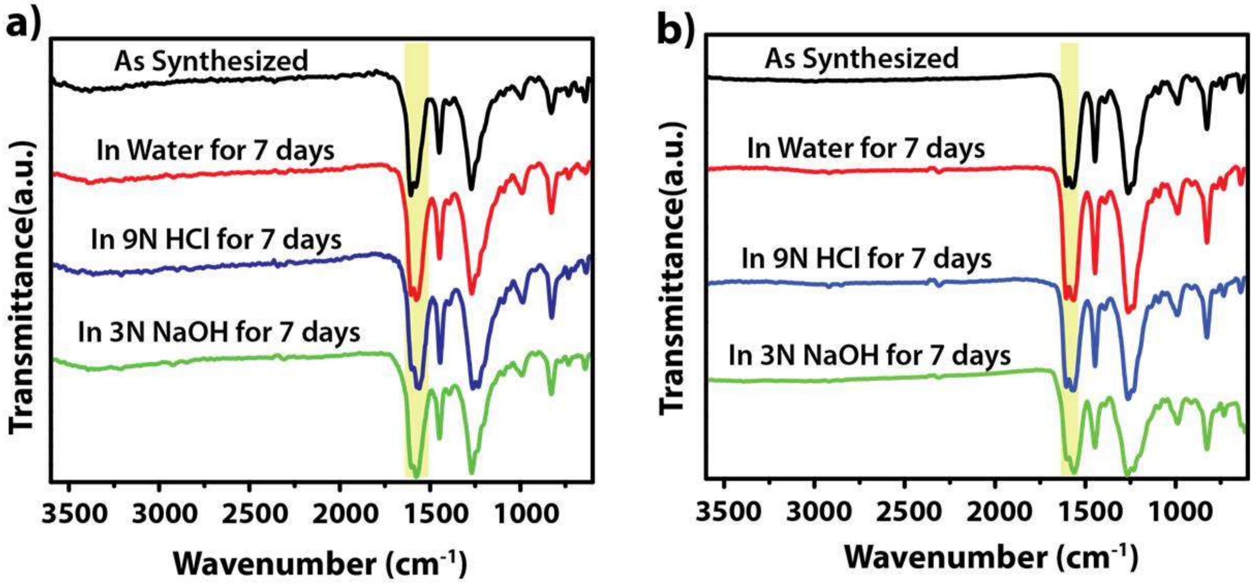

Figure S23: (a) FT-IR spectra recorded for **TpBpy-ST** as synthesized (Black), after water treatment (Red), acid treatment (Blue) and base treatment (Green); (b) FT-IR spectra recorded for **TpBpy-MC** as synthesized (Black), after water treatment (Blue), acid treatment (Red) and base treatment (Green).

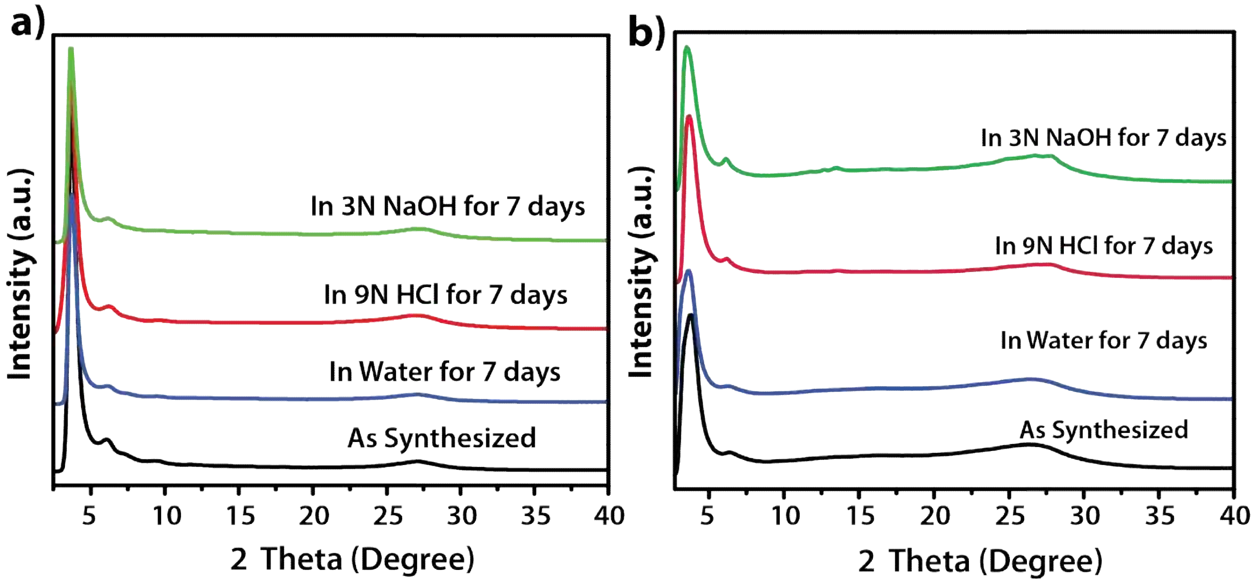

Figure S24: (a) PXRD recorded for **TpBpy-ST** as synthesized (Black), after water treatment (Blue), acid treatment (Red) and base treatment (Green); (b) PXRD recorded for **TpBpy-MC** as synthesized (Black), after water treatment (Blue), acid treatment (Red) and base treatment (Green).

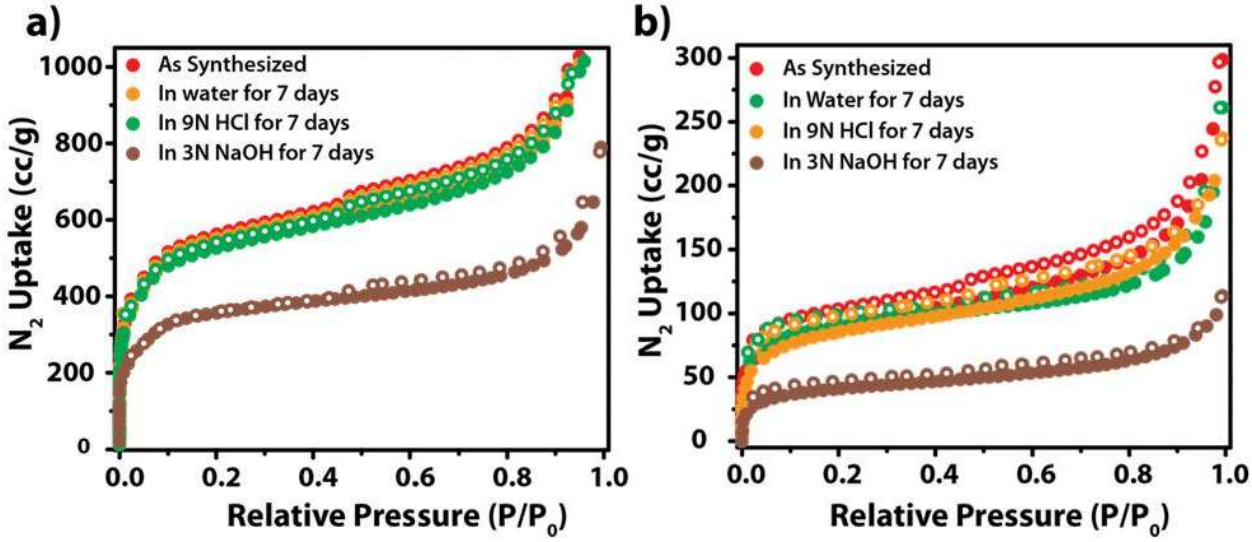

Figure S25: (a) N_2 sorption isotherms recorded for **TpBpy-ST** before (Red), after water treatment (Orange), acid treatment (Green) and base treatment (Brown) studies; (b) N_2 sorption isotherms recorded for **TpBpy-MC** before (Red), after water treatment (Orange), acid treatment (Green) and base treatment (Brown) studies.

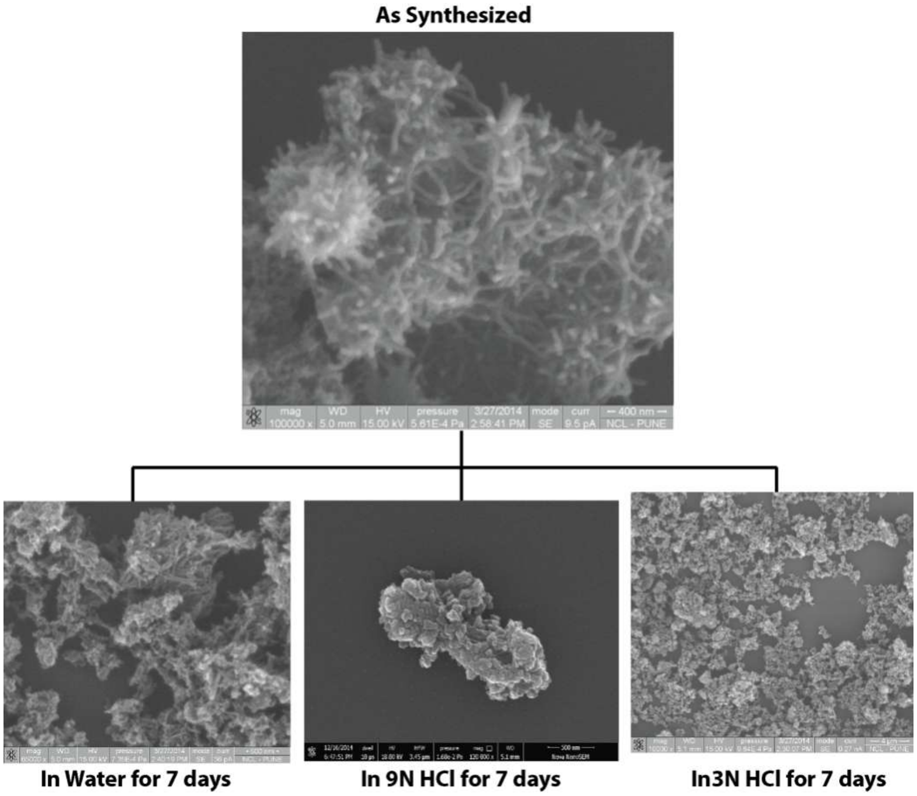

As Synthesized

In Water for 7 days

In 9N HCl for 7 days

In3N HCl for 7 days

Figure S26: SEM images of **TpBpy-ST** before and, after water, acid and base treatment.

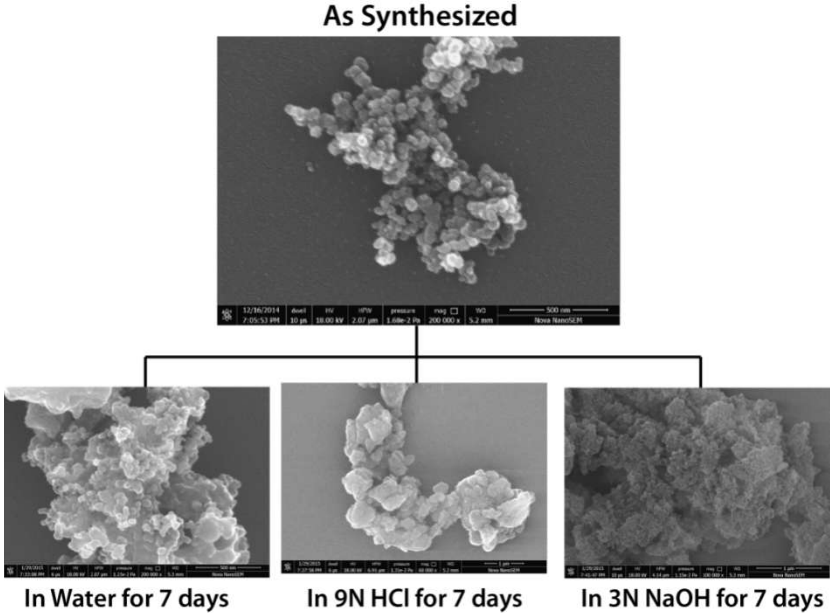

As Synthesized

In Water for 7 days

In 9N HCl for 7 days

In 3N NaOH for 7 days

Figure S27: SEM images of **TpBpy-MC** before and after water, acid and base treatment.

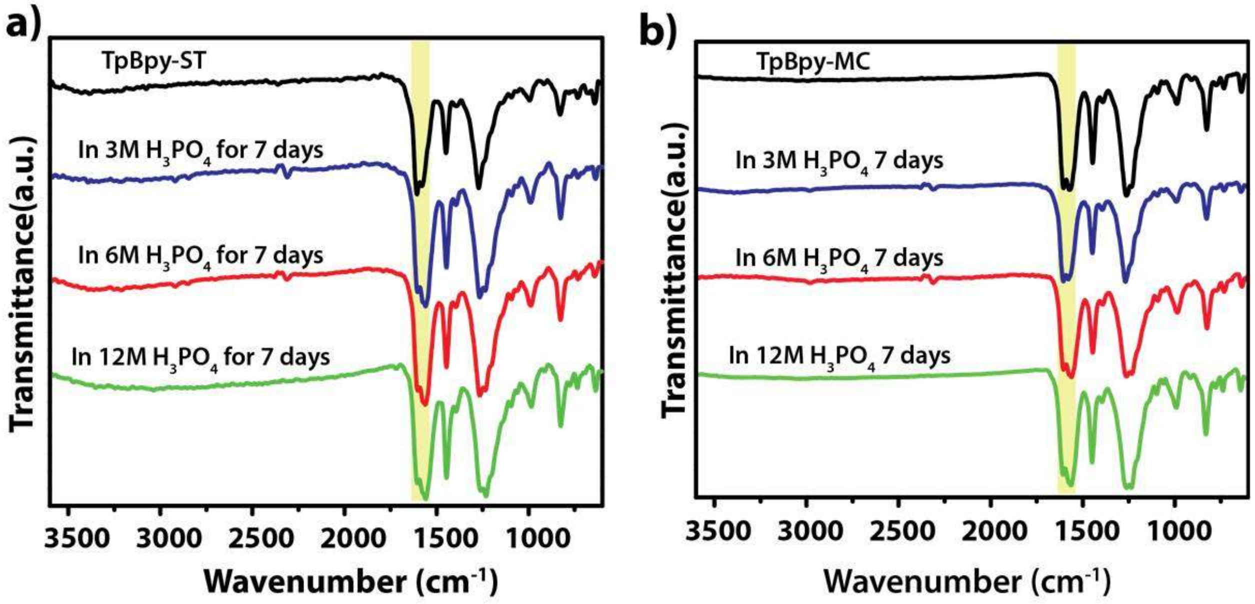

Figure S28: (a) FT-IR spectra recorded for **TpBpy-ST** as synthesized (Black), after treatment in 3M H_3PO_4 (Blue), 6M H_3PO_4 (Red) and 12M H_3PO_4 (Green); (b) FT-IR spectra recorded for **TpBpy-MC** as synthesized (Black), after treatment in 3M H_3PO_4 (Blue), 6M H_3PO_4 (Red) and 12M H_3PO_4 (Green).

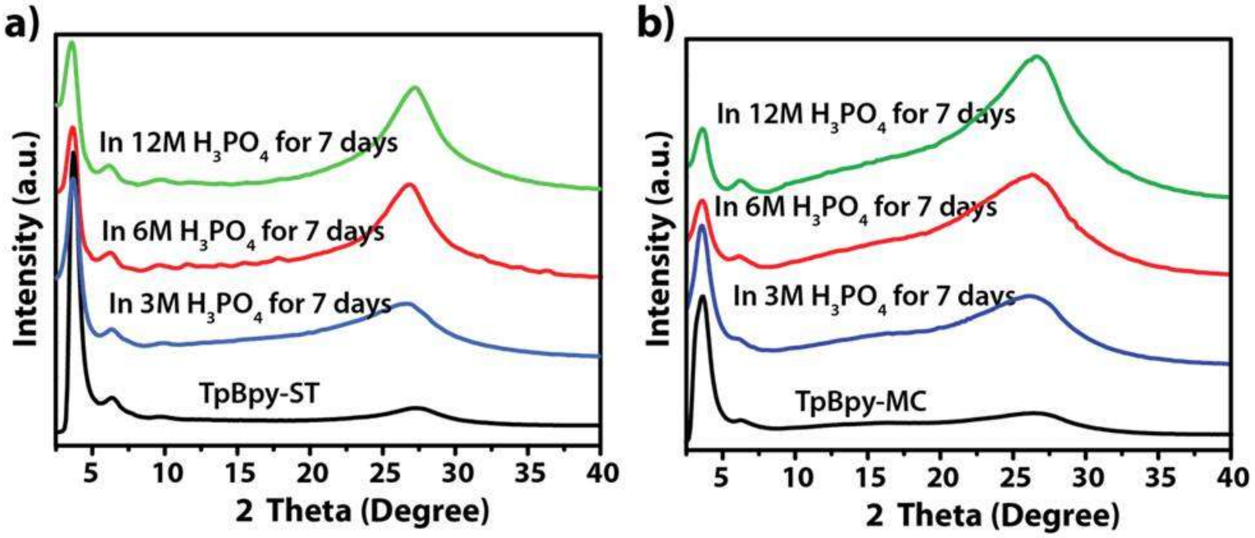

Figure S29: (a) PXRD recorded for **TpBpy-ST** as synthesized (Black), after treatment in 3M H_3PO_4 (Blue), 6M H_3PO_4 (Red) and 12M H_3PO_4 (Green); (b) PXRD recorded for **TpBpy-MC** as synthesized (Black), after treatment in 3M H_3PO_4 (Blue), 6M H_3PO_4 (Red) and 12M H_3PO_4 (Green).

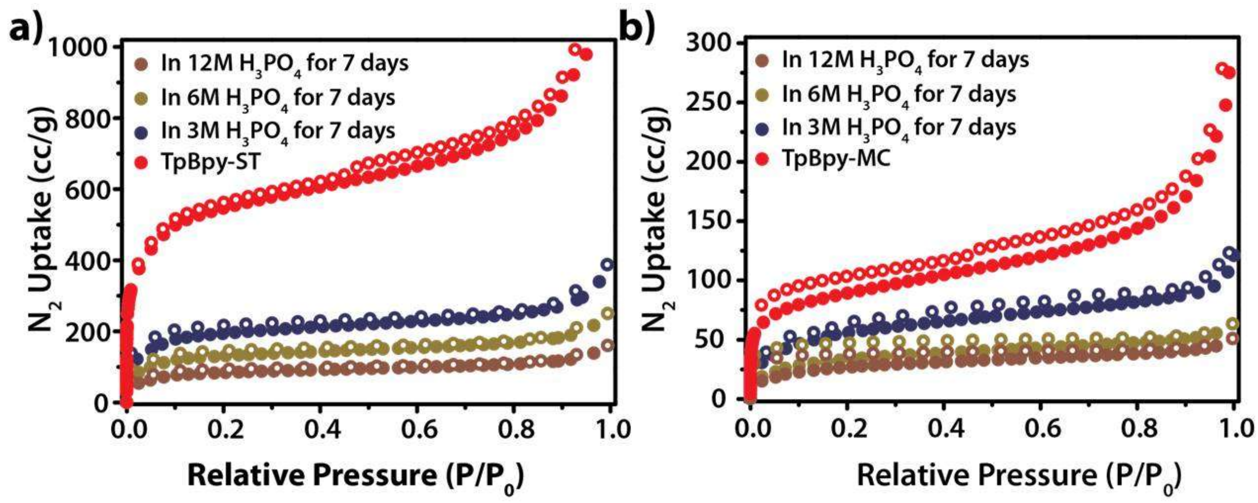

Figure S30: (a) N_2 sorption isotherms recorded for **TpBpy-ST** before (Red), after treatment in 3M H_3PO_4 (Blue), 6M H_3PO_4 (Dark Yellow) and 12M H_3PO_4 (Wine); (b) N_2 sorption isotherms recorded for **TpBpy-MC** as synthesized (Red), after treatment in 3M H_3PO_4 (Blue), 6M H_3PO_4 (Dark Yellow) and 12M H_3PO_4 (Wine).

Section S-11: X-ray investigation of single crystals of PA@Bpy

Table S3: Crystal data and structure refinement for 2,2'-bipyridinium-5-amino-5'-ammonium bis-dihydrogen phosphate

Identification code	2,2'-bipyridinium-5-amino-5'-ammonium bis-dihydrogen phosphate
Empirical formula	$C_{10}H_{16}N_4O_8P_2$
Formula weight	382.21
Temperature/K	298
Crystal system	triclinic
Space group	P-1
a/Å	8.6237(9)
b/Å	8.9142(10)
c/Å	10.2301(8)
α/°	73.441(9)
β/°	85.209(8)
γ/°	83.669(9)
Volume/Å^3	748.10(13)
Z	2
ρ_{calc}mg/mm^3	1.692
m/mm^{-1}	0.343
F(000)	396.0
Crystal size/mm^3	0.4 × 0.2 × 0.2

2Θ range for data collection	6.14 to 58.16°
Index ranges	-11 ≤ h ≤ 11, -11 ≤ k ≤ 12, -13 ≤ l ≤ 13
Reflections collected	5795
Independent reflections	3425[R(int) = 0.0246]
Data/restraints/parameters	3425/0/236
Goodness-of-fit on F^2	1.054
Final R indexes [I>=2σ (I)]	R_1 = 0.0414, wR_2 = 0.0980
Final R indexes [all data]	R_1 = 0.0507, wR_2 = 0.1066
Largest diff. peak/hole / e $Å^{-3}$	0.41/-0.42

Cambridge Crystallographic Data Centre Identifier: CCDC 1046997

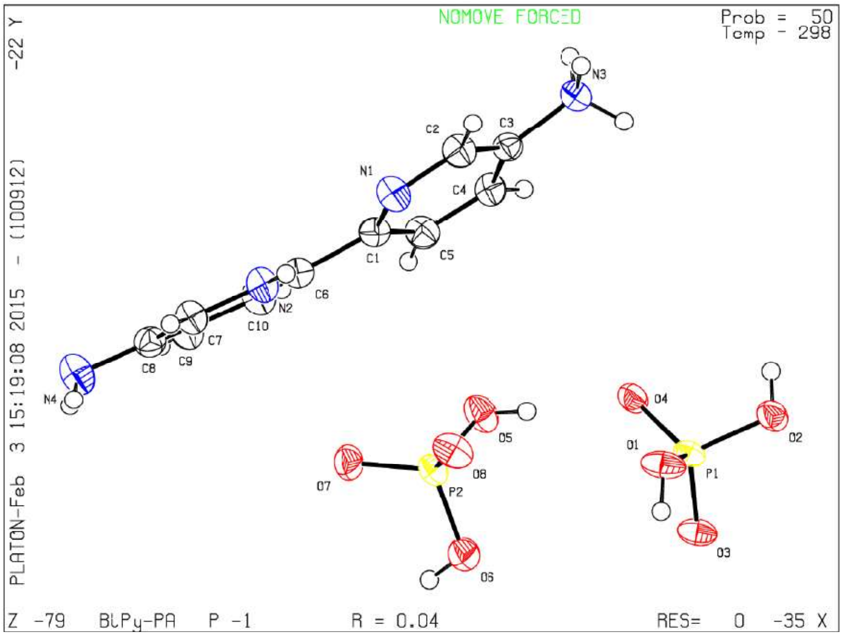

Figure S31: ORTEP diagram of 2,2'-bipyridinium-5-amino-5'-ammonium bis-dihydrogen phosphate with thermal ellipsoids at 50% probability.

Table S4: Crystal data and structure refinement for 2,2'-bipyridinium-5,5'-diamino hydrogen phosphate monohydrate

Identification code	2,2'-bipyridinium-5,5'-diamino hydrogen phosphate monohydrate
Empirical formula	$C_{10}H_{15}N_4O_5P$
Formula weight	302.23
Temperature/K	298
Crystal system	monoclinic
Space group	$P2_1/n$
a/Å	12.9672(5)

b/Å	4.22937(14)
c/Å	24.0975(8)
α/°	90.00
β/°	100.972(4)
γ/°	90.00
Volume/Å^3	1297.42(8)
Z	4
ρ_{calc}mg/mm^3	1.547
m/mm^{-1}	0.239
F(000)	632.0
Crystal size/mm^3	0.4 × 0.3 × 0.2
2Θ range for data collection	6.4 to 57.86°
Index ranges	$-17 \le h \le 16$, $-5 \le k \le 5$, $-30 \le l \le 29$
Reflections collected	5075
Independent reflections	2944[R(int) = 0.0223]
Data/restraints/parameters	2944/0/277
Goodness-of-fit on F^2	1.084
Final R indexes [I>=2σ (I)]	$R_1 = 0.0465$, $wR_2 = 0.1138$
Final R indexes [all data]	$R_1 = 0.0555$, $wR_2 = 0.1205$
Largest diff. peak/hole / e Å^{-3}	0.29/-0.26

Cambridge Crystallographic Data Centre identifier: CCDC 1046996

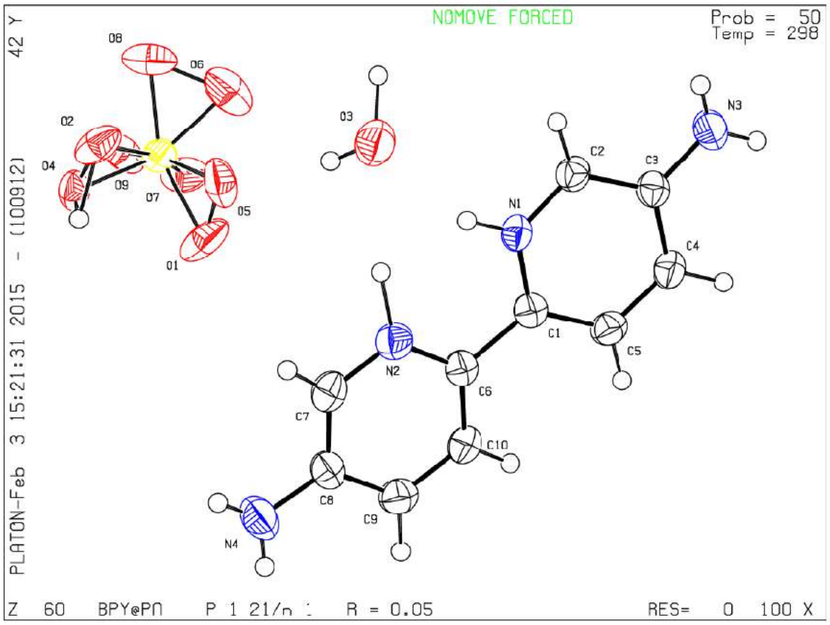

Figure S32: ORTEP diagram of 2,2'-bipyridinium-5,5'-diamino hydrogen phosphate monohydrate with thermal ellipsoids at 50% probability.

Section S-12: UV-Vis spectra

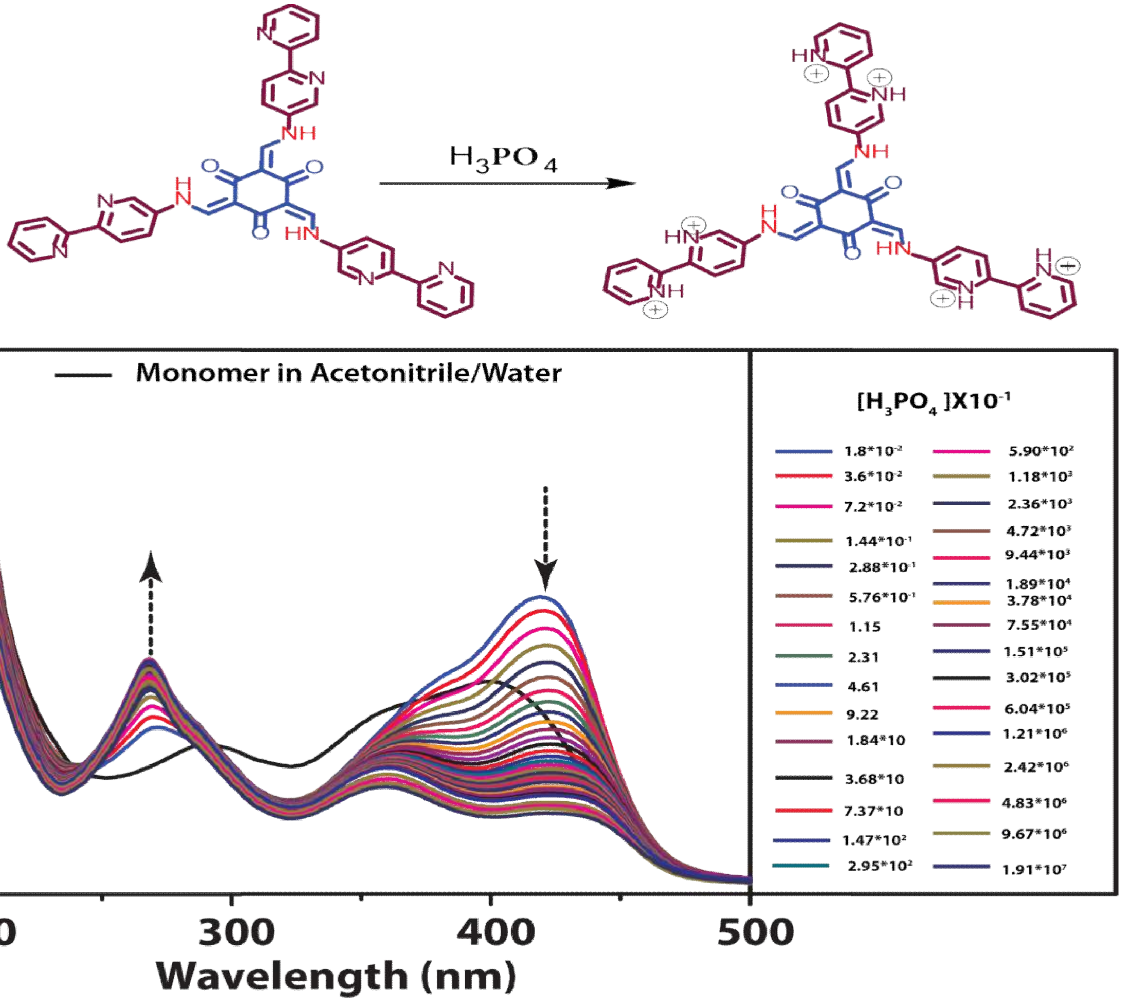

Figure S33: Changes in the absorption spectra of monomer with increasing concentration of H_3PO_4.

Section S-13: Phosphoric acid loading in TpBpy

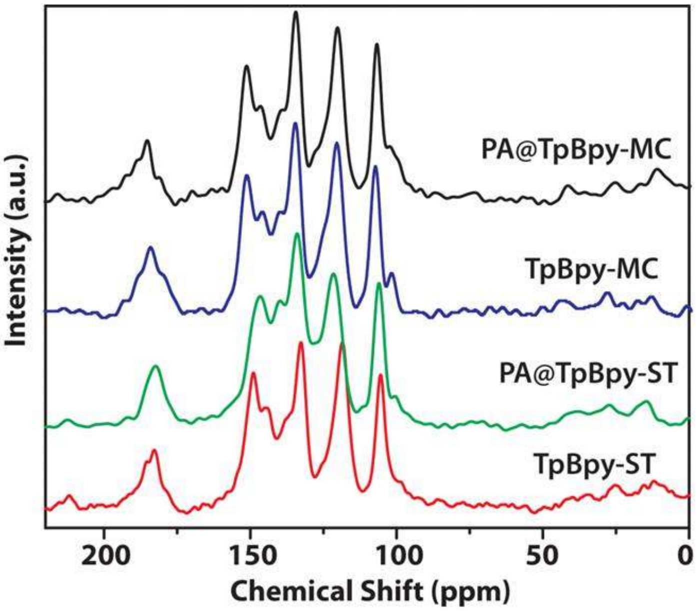

Figure S34: ^{13}C CP-MAS spectrum of **TpBpy-ST** (Red), **PA@TpBpy-ST** (Green), **TpBpy-MC** (Blue) and **PA@TpBpy-MC** (Black).

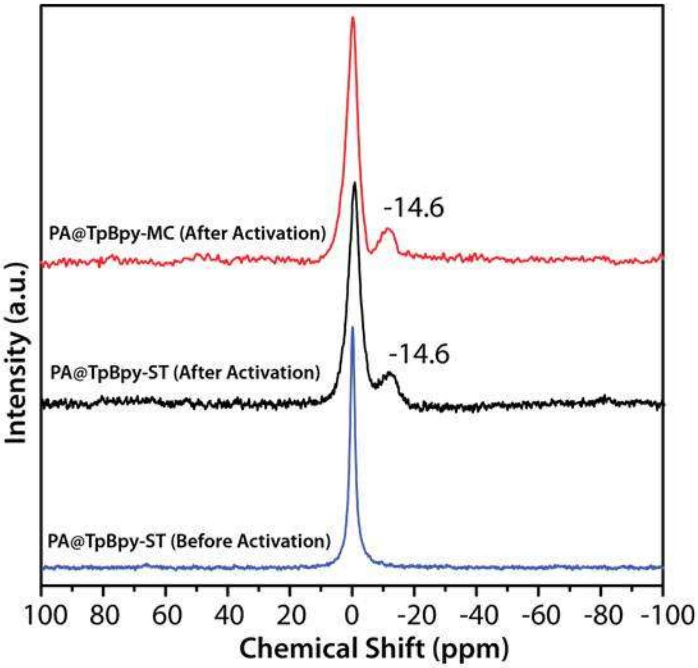

Figure S35: ^{31}P CP-MAS spectrum of **PA@TpBpy-ST (Before Activation),** (Blue) **PA@TpBpy-ST (After Activation)** (Red) and **PA@TpBpy-MC (After Activation)** (Black).

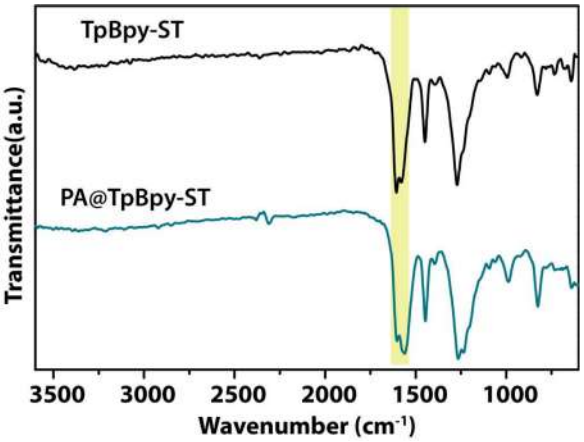

Figure S36: FT-IR spectra recorded **TpBpy-ST** as synthesized (Black), and **PA@TpBpy-ST** (Green).

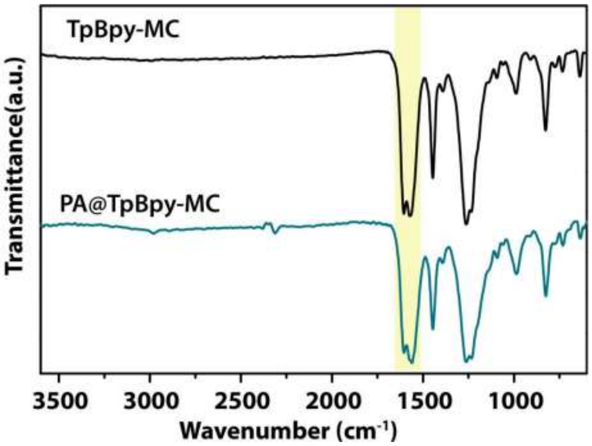

Figure S37: FT-IR spectra recorded **TpBpy-MC** as synthesized (Black) and **PA@TpBPy-MC** (Cyan).

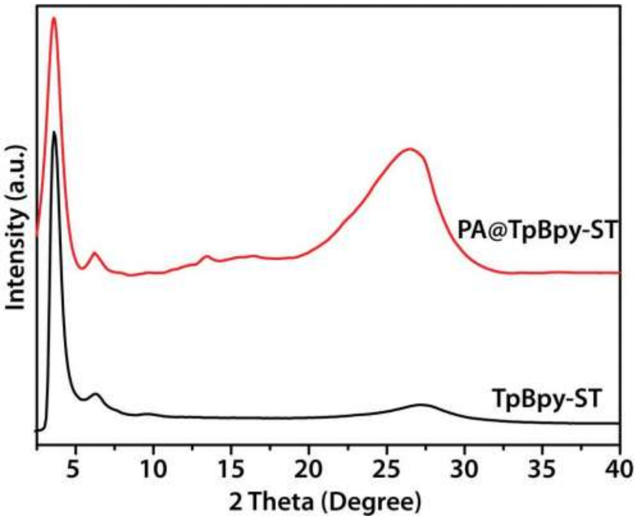

Figure S38: PXRD recorded for **TpBpy-ST** and **PA@TpBpy-ST**.

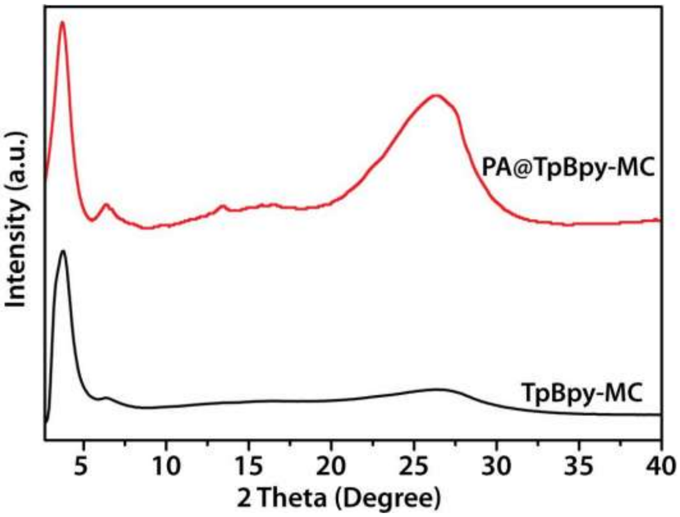

Figure S39: PXRD recorded for **TpBpy-MC** and **PA@TpBpy-MC**.

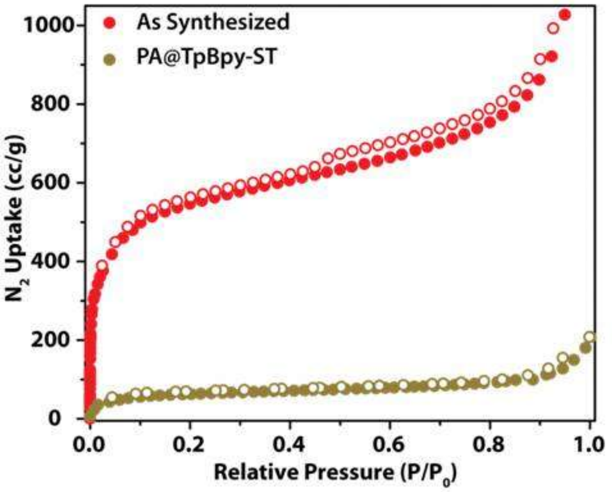

Figure S40: N_2 sorption isotherms recorded for **TpBpy-ST** before (Red) and **PA@TpBpy-ST** (Yellow).

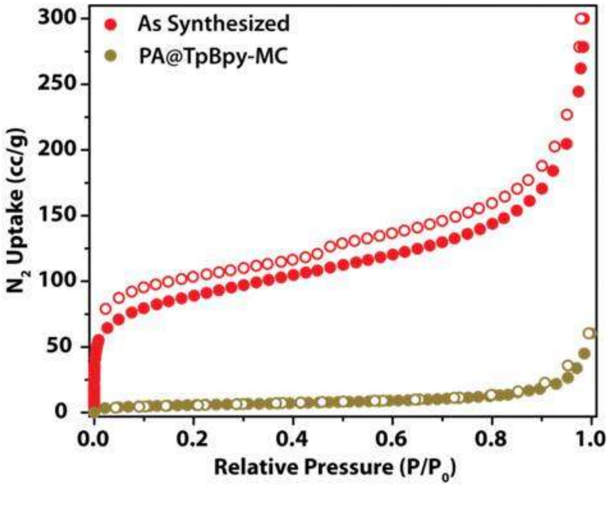

Figure S41: N_2 sorption isotherms recorded for **TpBpy-MC** before (Red) and **PA@TpBpy-MC** (Yellow).

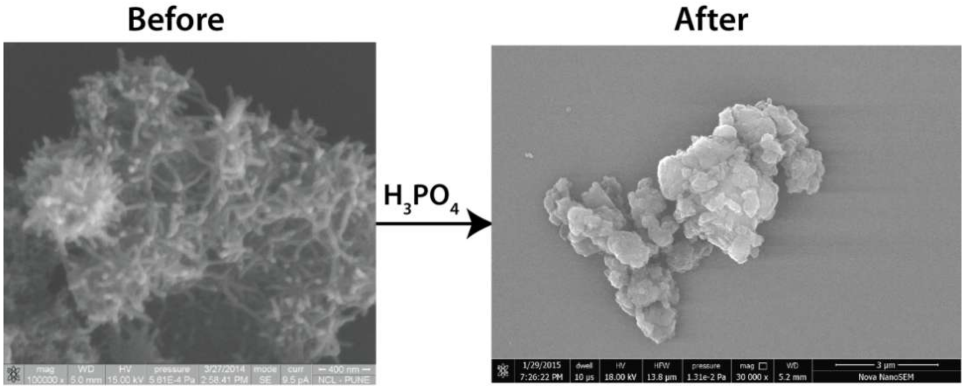

Figure S42: SEM images of **TpBpy-ST** (before) and **PA@TpBpy-ST** (after 12 M H_3PO_4 for 2 h treatment).

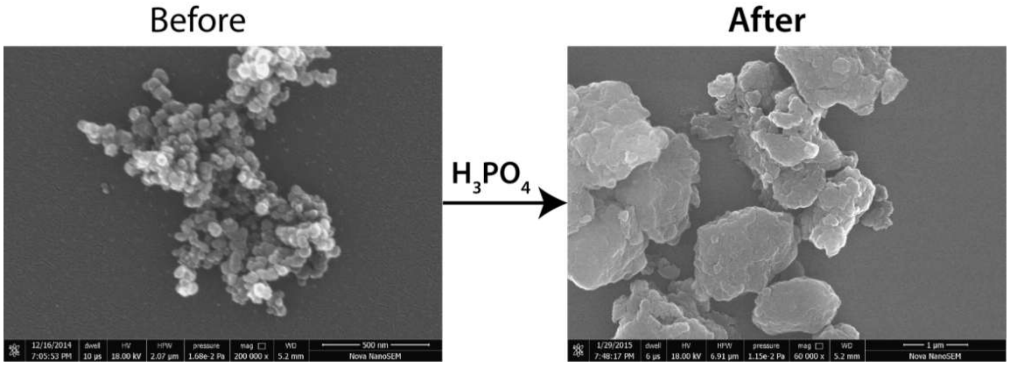

Figure S43: SEM images of **TpBpy-MC** (before) and **PA@TpBpy-MC** (after 12 M H_3PO_4 for 2 h treatment).

Section S-14: Proton Conductivity Studies of COFs

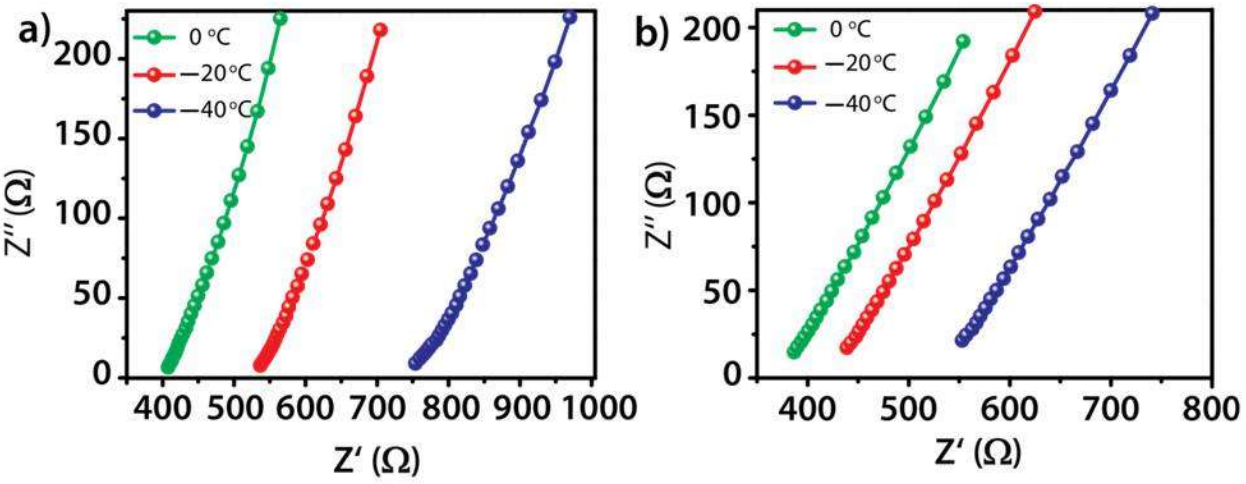

Figure S44: The proton conductivity spectra of a) **PA@TpBpy-ST** and b) **PA@TpBpy-MC** under low temperature.

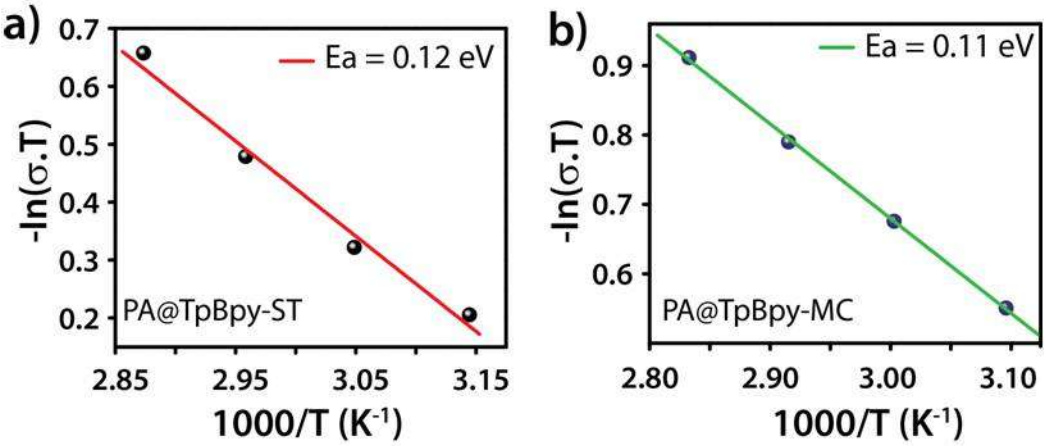

Figure S45: Activation energy fitting for (a) **PA@TpBpy-ST** and (b) **PA@TpBpy-MC.**

Table S5: Proton conductivity data of PA@TpBpy-ST and –MC under low temperature.

Sl. No	**Temperature (in °C)**	**Proton Conductivity of PA@TpBpy-ST ($S.cm^{-1}$)**	**Proton Conductivity of PA@TpBpy-MC ($S.cm^{-1}$)**
1	0	2.77 X 10^{-4}	3.16 X 10^{-4}
2	-20	2.29 X 10^{-4}	2.44 X 10^{-4}
3	-40	1.53 X 10^{-4}	1.92 X 10^{-4}

Table S6: Proton conductivity data of reported MOFs and COFs.

Sr. No	Compound Name	Conductivity (S/cm)	Ea	Conditions	*References*
1	His@$[Al(OH)(ndc)]_n$	1.7×10^{-3}	0.25	150 °C, Anhydrous	*Angew. Chem. Int. Ed. 2011, 50, 11706.*
2	β-PCMOF-2$(Tz)_{0.45}$	5.0×10^{-4}	0.34	150 °C, Anhydrous	*Nat. Chem. 2009, 1, 705.*
3	In-IA-2D-2	1.2×10^{-5}	0.48	90 °C, Anhydrous	*Chem. Commun. 2013, 49, 6197.*
4	Im@$\{Al(\mu_2\text{-}OH)(1,4\text{-}bdc)\}_n$	2.2×10^{-5}	0.90	120 °C, Anhydrous	*Nat. Mater. 2009, 8, 831.*
5	H_2SO_4@MIL-101	1.0×10^{-2}	0.42	150 °C, 0.13% RH	*J. Am. Chem. Soc. 2012, 134, 15640.*
6	**PA@TpBpy-ST**	**1.98×10^{-3}**	**0.12**	**120 °C**	**Present work**
7	**PA@TpBpy-MC**	**2.50×10^{-3}**	**0.11**	**120 °C**	**Present work**
8	PA@Tp-Azo	6.7×10^{-5}	0.11	67 °C, Anhydrous	*J. Am. Chem. Soc. 2014, 136, 6570.*
9	$[Zn_3(H_2PO_4)_6](Hbim)$	1.3×10^{-3}	0.50	120 °C, Anhydrous	*J. Am. Chem. Soc. 2013, 135, 11345.*
10	Im@Td-PPI 2	3.49×10^{-4}	0.30	90 °C, Anhydrous	*J. Am. Chem. Soc. 2015, 137, 913.*
11	$[ImH_2][Cu(H_2PO_4)_{1.5}(HPO_4)_{0.5} \cdot Cl_{0.5}]$	2.0×10^{-2}	1.10	130 °C, Anhydrous	*Chem. Commun. 2014, 50, 10241.*
12	$[Zn(HPO_4)(H_2PO_4)_2]\ (ImH_2)_2$	2.5×10^{-4}	0.47	130 °C, Anhydrous	*J. Am. Chem. Soc. 2012, 134, 7612.*
13	H_3PO_4@MIL-101	3.0×10^{-3}	0.25	150 °C, 0.13% RH	*J. Am. Chem. Soc. 2012, 134, 15640.*
14	$\{[(Me_2NH_2)_3(SO_4)]_2[Zn_2(ox)_3]\}_n$	1.0×10^{-4}	0.13	150 °C, N_2 atmosphere	*Angew. Chem. Int. Ed. 2014, 53, 2638.*

Section S-15: MEA Studies

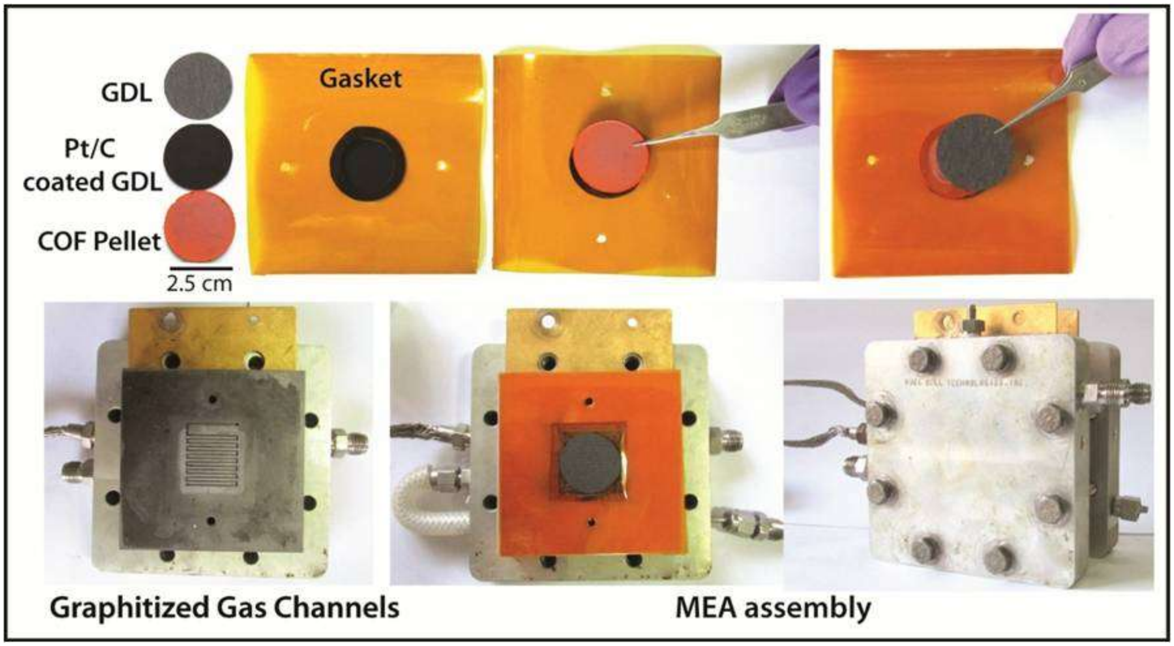

Figure S46. Optical photograph of the fuel cell assembly using fabricated MEA with pelletized **PA@TpBpy** COF as solid electrolyte.

MEA fabrication was performed using the standard PEFMC protocol. Initially, ca. ~250 mg of COF powder was pelletized using 2.5 mm diameter die. The fuel cell electrodes were prepared by spraying the Pt catalyst ink onto the porous carbon paper (35CC-SGL with 15% PTFE content). The COF pellet was then placed between two platinized carbon electrodes [each containing Pt catalyst (Johnson Matthey) + Vulcan carbon support (VX 72) + Nafion binder (20%)] using Kapton gasket. The entire assembly was then cold pressed applying 1000 KgN pressure for 2 min. The MEA was then arranged onto the graphite plates using FRT gasket for single cell assembly (active area = 4 cm^2, Fuel cell Tech).

The single cell test fixture used for fuel cell polarization study consists of following components:

- *Aluminium end-plates*

- *Graphite mono polar plates provided with integrated O-ring gasket and serpentine gas flow field*
- *Cathode loading:* 1 mg/cm^2; N/C: 0.4; electrode thickness: 349 µm
- *Anode loading:* 1 mg/cm^2; N/C: 0.4; electrode thickness: 351 µm
- *Gas flow:* 0.5 slpm for anode as well as cathode.
- *Operating temperature:* RT-50 ˚C
- *Membrane pellet thickness:* 850± 5 µm
- *MEA thickness:* 1558 ± 5 µm
- *Thickness of Gasket used :* 630 µm

Electromotive force studies (EMF) of fabricated Membrane Electrode Assembly (MEA):

The cell was fed with pure dry hydrogen (99.999%) at anode and pure dry O_2 (99.9%) for EMF measurements. In case of solvothermally synthesized COF derived pellet, the cell showed a starting OCV of 0.66 V at 30 °C. On increasing the temperature to 50°C, the OCV increased slightly to 0.68V, before decreasing rapidly thereby forcing the cell shut down. On the other hand, in case of mechanochemically derived COF, the cell showed a starting Open Circuit Voltage (OCV) of 0.86 ± 0.02V at 30°C. On further increasing the temperature, the OCV shoot up to 0.92 ± 0.02V at 50°C and remained constant thereafter. The OCV was observed to remain stable for the next 2.5 h, which confirmed the denser nature of the mechanochemically synthesized COF pellet.

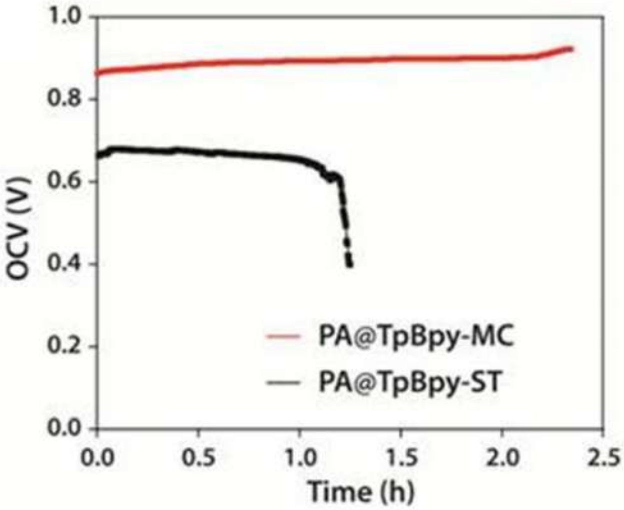

Figure S47. Lifetime measurement of OCV obtained using the fabricated MEA.

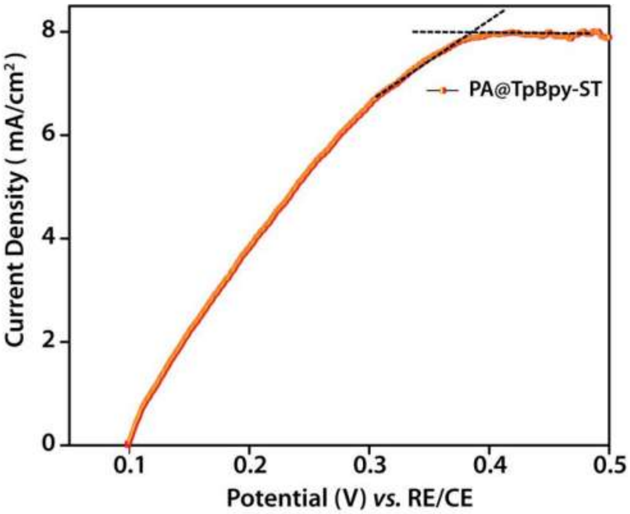

Figure S48. Linear Sweep voltammogram for hydrogen cross over in **PA@TpBpy-ST** constituted PEMFC after 1.2 h of OCV life test measurement.

The cell was found to exhibit a mass transfer limited current density (J_{lim}) of 8 mA cm^{-2} at 50 °C. This limiting current is proportional to the rate of H_2 cross over from anode to cathode as given by the relation, [6]

$$J_{\text{x-over, H2}} = J_{\text{lim}} / nF$$

where, $n = 2$ for H_2 oxidation reaction and F is Faraday's constant= 96485 C/electron-mole.

Using this relation, the H_2 crossover flux at the cathode was calculated to be $\underline{4.1 \times 10^{-8}\ \text{mol cm}^{-2}\ \text{s}^{-1}}$ at 50°C. This value is found to be nearly one order higher than that reported for pristine MEAs derived from Nafion as the proton conducting membrane (normally, in the order of 10^{-9} mol cm^{-2} s^{-1}).

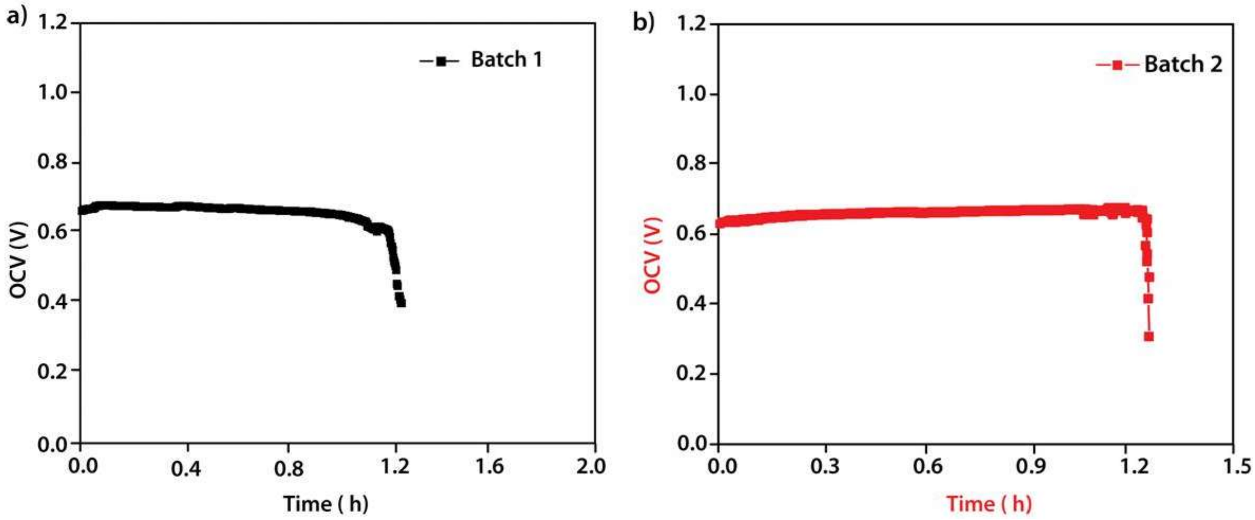

Figure S49. OCV life test profiles of MEA fabricated using two different batches a) and b) of **PA@TpBpy-ST** pellet to check data reproducibility.

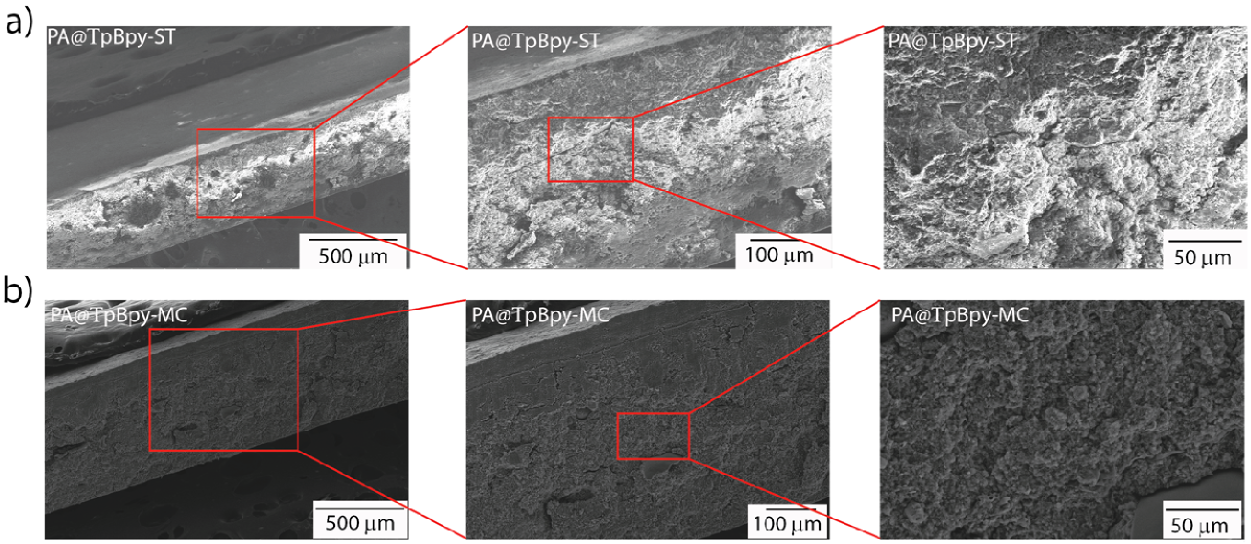

Figure S50: a) Cross Section of pellets **PA@TpBpy-ST,** its zoomed section and b) Cross Section of pellets **PA@TpBpy-MC** and its zoomed section.

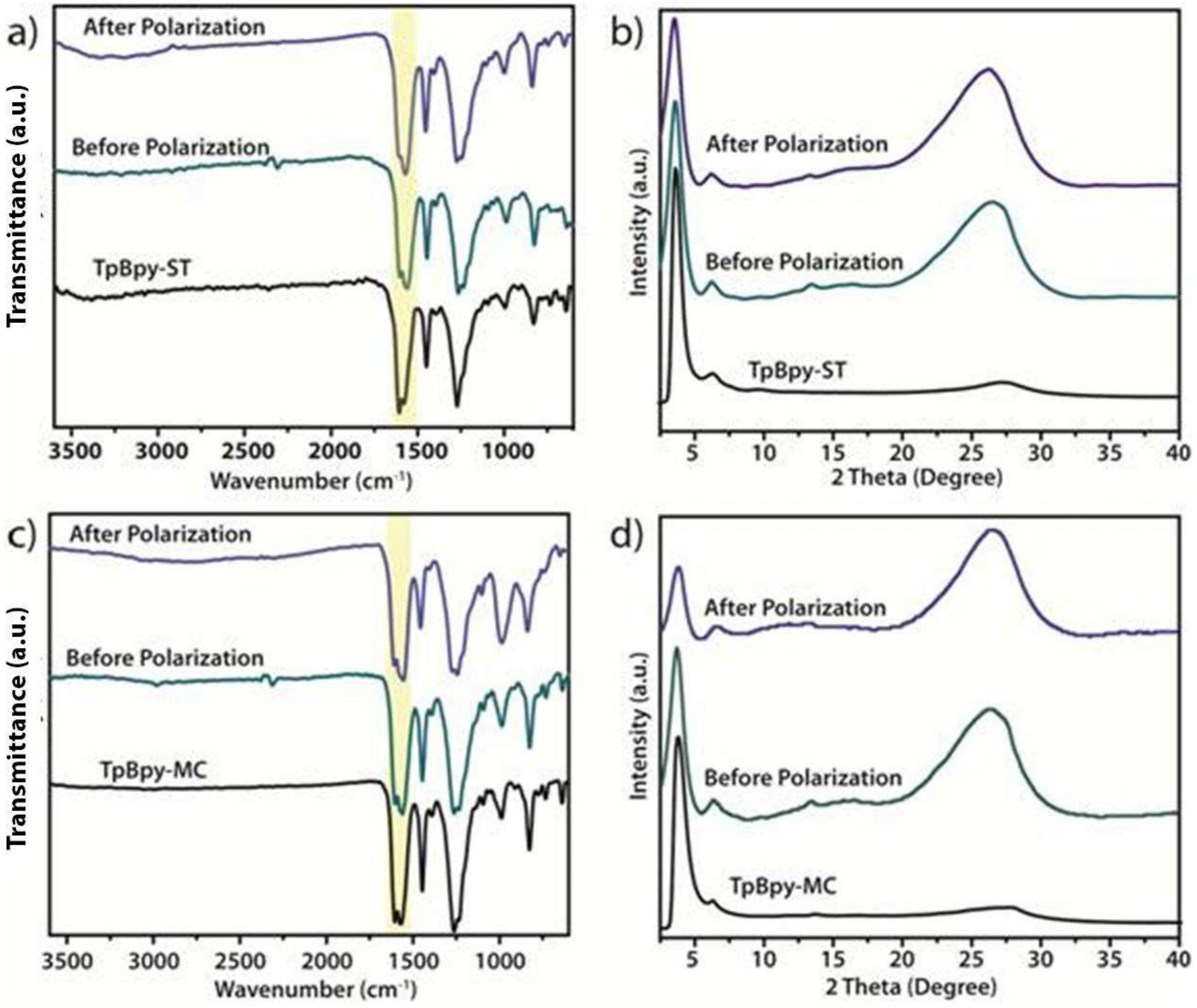

Figure S51: a) FT-IR spectra recorded **TpBpy-ST** (Black), before polarization (Green) and after polarization (Blue) using **PA@TpBpy-ST** b) PXRD recorded for **TpBpy-ST** (Black), before polarization (Green) and after polarization (Blue) using **PA@TpBpy-ST** c) FT-IR spectra recorded **TpBpy-MC** (Black), before polarization (Green) and after polarization (Blue) **PA@TpBpy-MC** and PXRD recorded for **TpBpy-ST** (Black), before polarization (Green) and after polarization (Blue) **PA@TpBpy-MC**.

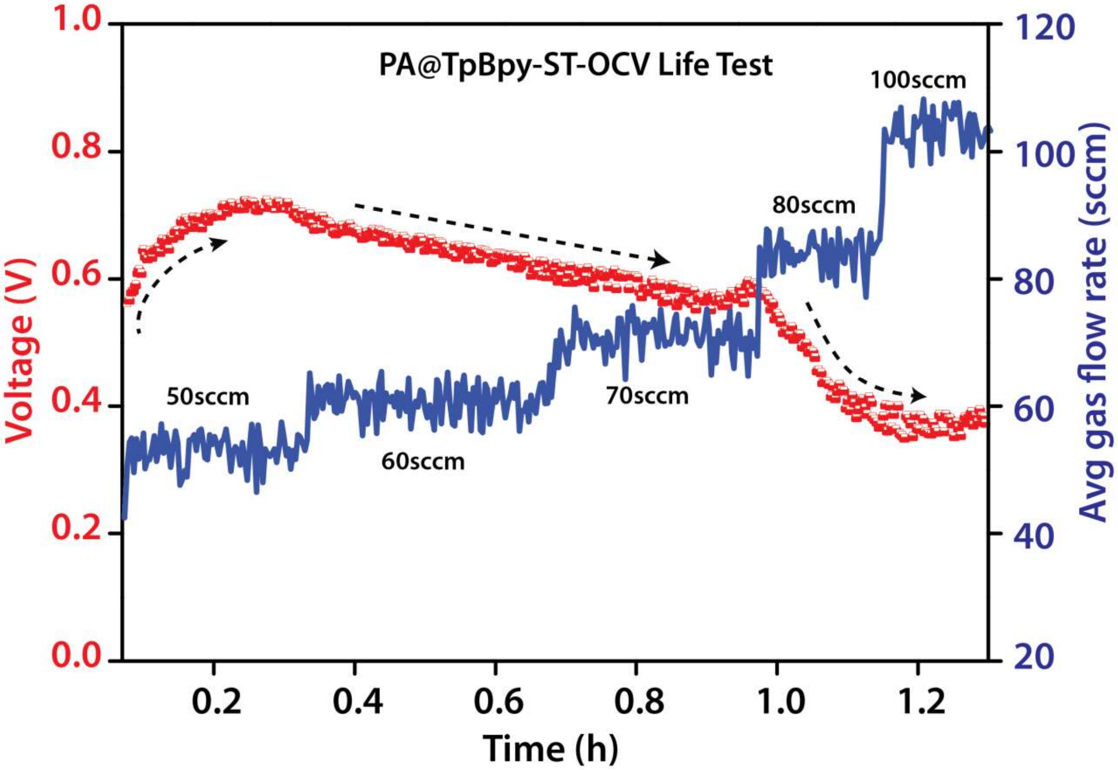

Figure S52. Study of effect of flow rate on OCV of **PA@TpBpy-ST** constituted MEA at 50 ^{o}C.

In situ Impedance study on the fabricated Membrane Electrode Assembly (MEA)

The *in situ* impedance measurements was carried out *via* two electrode configuration using *BioLogic* VPM3 electrochemical work station in the frequency range of 1 MHz – 100 Hz and 10 mV input voltage amplitude, with O_2 passing cathode used as working electrode and H_2 passing anode as counter and reference electrodes. The results were studied using Nyquist plots obtained at each temperature (from 30-50 ˚C).The plots were then fit using a PEFMC fuel cell equivalent circuit and the electrolyte resistance was calculated determined by the intercept made on the real axis at the high frequency regime in the complex impedance plane.

Following equivalent circuit was used for fitting the experimental data:

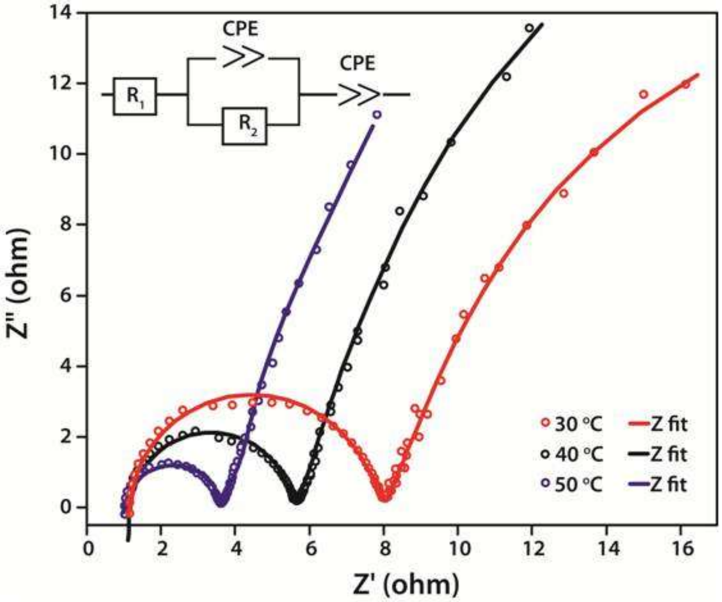

Figure S53. Nyquist plots obtained at different temperatures (in ˚C) with equivalent circuit used for fitting (inset).

wherein,

R_1 = Solid electrolyte resistance,
R_2 = Charge transfer resistance at electrode-electrolyte interface,
CPE = Constant Phase Element.

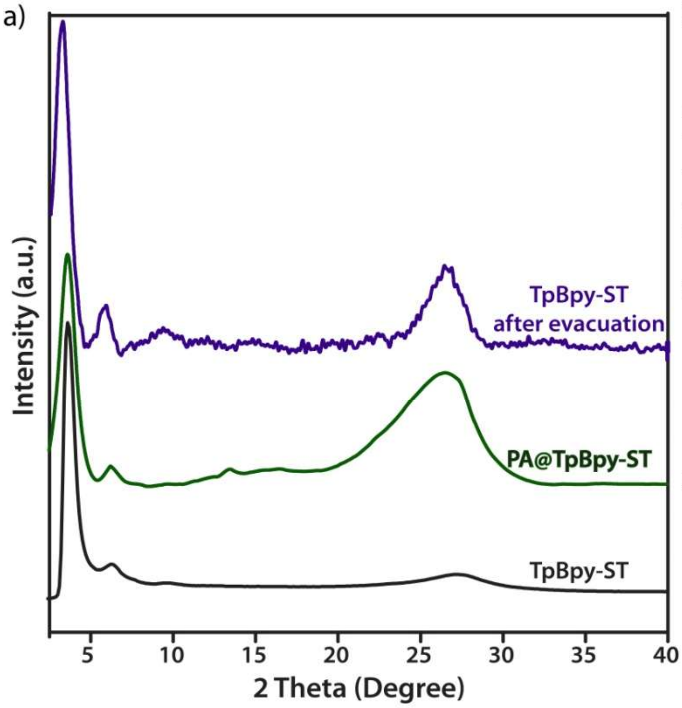

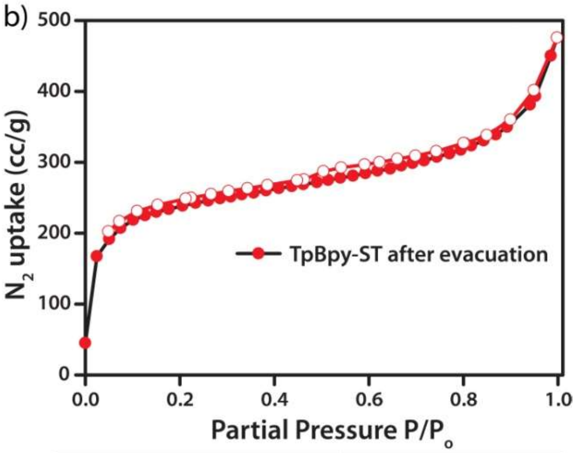

c)

Sample	BET Surface area (m^2/g)
TpBpy-ST	1746
PA@TpBpy-ST	203
TpBpy-ST after evacuation	750

Figure S54. a) Comparative PXRD spectra indicating the restoration of the TpBpy-ST COF's porous nature after evacuating phosphoric acid from its pores b) N_2 adsorption isotherm of TpBpy after evacuation of phosphoric acid from its pores (below) c) Table comparing the surface area after evacuation process.

Section S-16: References

1) J. H. Chong, M. Sauer, B. O. Patrick and M. J. MacLachlan, *Org. Lett.*, 2003, **5**, 3823.
2) M. Albrecht, I. Janser, A. Lützen, M. Hapke, R. Fröhlich and P. Weis, *Chem. Eur. J.*, 2005, **11**, 5742.
3) C. R. DeBlase, K. E. Silberstein, T. -T. Truong, H. D. Abruña and W. R. Dichtel, *J. Am. Chem. Soc.*, 2013, **135**, 16821.
4) B. Lukose, A. Kuc and T. Heine, *Chem. Eur. J.*, 2011, **17**, 2388.
5) Accelrys, Material Studio Release Notes, Release 4.2, Accelrys Software, San Diego 2006.
6) a) A. J. Bard and L. Faulkner, John Wiley & Sons: New York, NY (2001); b) M. Schoemaker, U. Misz, P. Beckhaus and A. Heinzel, *Fuel Cells*, 2014, **14**,412.